

A PROBABILISTIC APPROACH TO TRAJECTORY-BASED OPTIMAL EXPERIMENTAL DESIGN*

AHMED ATTIA[†]

Abstract. We present a novel probabilistic approach for optimal path experimental design. In this approach a discrete path optimization problem is defined on a static navigation mesh, and trajectories are modeled as random variables governed by a parametric Markov policy. The discrete path optimization problem is then replaced with an equivalent stochastic optimization problem over the policy parameters, resulting in an optimal probability model that samples estimates of the optimal discrete path. This approach enables exploration of the utility function's distribution tail and treats the utility function of the design as a black box, making it applicable to linear and nonlinear inverse problems and beyond experimental design. Numerical verification and analysis are carried out by using a parameter identification problem widely used in model-based optimal experimental design.

Key words. Path experimental design, Probabilistic optimization, Trajectory optimization Bayesian inference.

AMS subject classifications. 62K05, 35Q62, 62F15, 35R30, 35Q93, 65C60, 93E35

1. Introduction. Simulation models are critical for predicting the behavioral patterns of physical phenomena given the initial condition or the model state. These models, however, require calibration based on snapshots (observations) of the physical phenomena of concern. Inverse problems enable estimating the unknown model parameters from partial and noisy observations [3, 10, 11, 28]. Such observational data can be obtained from static observational sensors or moving sensors such as relocatable sensors and land and aerial vehicles such as drones and robots. Inverse problems underpin many applications, and their solution quality depends on data quality, making optimal data acquisition essential for accurate inference and prediction.

Model-based optimal experimental design (OED) [19, 30, 32] is the general mathematical formalism for optimizing the configuration of an experimental or observational setup in simulation systems. An experimental design $\zeta \in \Omega_\zeta$ encodes the decision variables such as the spatial distribution of observational instruments, the temporal frequency of data acquisition, or the trajectory of moving sensors. OED problems generally seek a design that “optimizes” some “utility function” $\mathcal{U}(\zeta)$ that quantifies the quality of the design ζ . The process includes *minimizing* the variance of an inference parameter estimator or *maximizing* the expected information gain [1, 6, 24].

Unlike OED for static sensor placement [1, 23], trajectory OED for mobile sensors remains underexplored. Most existing trajectory OED formulations [33, 38, 39] employ a parametrized form of the trajectory, such as ordinary differential equations, and follow a gradient-based optimization approach to tune the parameters of the trajectory. Although valuable, parametrized trajectory development confines solutions to

*Submitted to the editors January 19, 2026.

Funding: This material is based upon work supported by the U.S. Department of Energy, under contract number DE-AC02-06CH11357, with funding through, (1) Office of Science, Office of Advanced Scientific Computing Research: Scientific Discovery through Advanced Computing (SciDAC) Program through the FASTMath Institute; and (2) Competitive Portfolios Project on Energy Efficient Computing: A Holistic Methodology.

[†]Mathematics and Computer Science Division, Argonne National Lab, USA (aattia@anl.gov).

a specific trajectory family, limiting applicability. Moreover, incorporating hard constraints such as those imposed by the domain is a significant challenge. Additionally, this approach mandates development of utility- and observation-specific gradients.

Path planning for mobile sensors has been extensively investigated in applications such as robotics and autonomous vehicles; see, for example, [17, 21, 25–27, 29]. These methods are application-specific, however, and are not directly applicable to model-based OED. For example, graph-based path optimization [22] methods focus primarily on finding a minimum-cost path between two specific locations (nodes on a graph).

We propose a probabilistic path optimization framework with black-box utility functions, enabling out-of-the-box use with arbitrary criteria and observation patterns. Instead of providing only a single optimal path, this approach provides a probabilistic policy that samples near-optimal solutions, thereby enabling exploration of the tail (e.g., upper tail for maximization) of the OED utility function distribution.

Contributions. The main contributions of this work are summarized as follows.

1. We define the path OED problem as a discrete optimization problem over a graph. The discrete path problem is then reformulated as a stochastic optimization problem over probabilistic policy parameters, yielding an optimal probabilistic model.
2. We propose three probabilistic policy models based on first- and higher-order Markov chains, analyze their complexity–cost trade-offs, and derive stochastic optimization gradients with variance reduction.
3. We provide an efficient algorithmic approach for solving the probabilistic path optimization problem with emphasis on scalability to large-scale inverse problems.
4. All developments in this work are made publicly available through PyOED [18].

The rest of the paper is structured as follows. Section 2 presents an overview of the mathematical background of standard OED, and the generic probabilistic optimization framework. Section 3 describes the proposed path OED approach. Numerical results are in Section 4, and concluding remarks are given in Section 5.

2. Background: Model-Based OED.

An OED problem takes the form

$$(2.1) \quad \zeta^{\text{opt}} \in \arg \max_{\zeta \in \Omega_{\zeta}} \mathcal{U}(\zeta),$$

where $\zeta \in \Omega_{\zeta}$ is an experimental design variable that encodes tunable configurations of the system. Here, \mathcal{U} is a utility function—possibly application-dependent—that quantifies the quality of the design and generally requires multiple evaluations of the dynamical system in model-based OED problems. Typical choices of \mathcal{U} in Bayesian inference applications include the alphabetic criteria, such as A- and D-optimality [6, 39], which target minimizing posterior uncertainty of the inference parameter.

The design ζ in many OED problems is binary or discrete because it is typically associated with observational/experimental data that is generally defined on a finite domain. Solving the OED optimization problem (2.1) exactly is thus a major challenge. Greedy and exchange-type approaches [20, 40] have been traditionally followed for approximating the solution of (2.1) because of their simplicity and practical behavior. Convergence guarantees and scalability of such algorithms, however, are limited. Thus the optimization problem (2.1) is often replaced with an alternative formulation based on continuous relaxation of the design ζ . The relaxed formulation is then solved by following a gradient-based optimization approach, and the resulting design

is rounded to approximate the solution of [7]. This approach requires developing the gradient of the utility function with respect to the relaxed design $\nabla_{\zeta} \mathcal{U}$ and thus requires the utility function and any additional constraints such as sparsity-enforcing constraints, to be differentiable with respect to the relaxed design ζ .

2.1. Probabilistic Optimization Approach. We adopt the probabilistic optimization approach [8, 9], which replaces (2.1) with the policy optimization problem:

$$(2.2) \quad \mathbf{p}^{\text{opt}} \in \arg \max_{\mathbf{p}} \mathbb{E}_{\zeta \sim \mathbb{P}(\zeta | \mathbf{p})} [\mathcal{U}(\zeta)],$$

where ζ is modeled as a random variable with a parametric policy $\mathbb{P}(\zeta | \mathbf{p})$. A gradient ascent approach solves (2.2), yielding parameters \mathbf{p}^{opt} of an optimal policy from which $\zeta \sim \mathbb{P}(\zeta | \mathbf{p}^{\text{opt}})$ are sampled to approximate the original OED solution (2.1). A stochastic approximation of the gradient $\nabla_{\mathbf{p}} \mathbb{E}[\mathcal{U}(\zeta)]$ is employed to solve (2.2):

$$(2.3a) \quad \mathbf{g} = \nabla_{\mathbf{p}} \mathbb{E}_{\zeta \sim \mathbb{P}(\zeta | \mathbf{p})} [\mathcal{U}(\zeta)] = \mathbb{E}_{\zeta \sim \mathbb{P}(\zeta | \mathbf{p})} [\mathcal{U}(\zeta) \nabla_{\mathbf{p}} \log \mathbb{P}(\zeta | \mathbf{p})]$$

$$(2.3b) \quad \approx \frac{1}{N_{\text{ens}}} \sum_{k=1}^{N_{\text{ens}}} \mathcal{U}(\zeta[k]) \nabla_{\mathbf{p}} \log \mathbb{P}(\zeta[k] | \mathbf{p}) := \hat{\mathbf{g}},$$

with $\zeta[k] \sim \mathbb{P}(\zeta[k] | \mathbf{p})$, $k = 1, \dots, N_{\text{ens}}$, sampled from the parametric policy. Because only evaluations of \mathcal{U} at sampled designs are required, the probabilistic approach (2.2) is applicable to black-box objectives \mathcal{U} .

This probabilistic approach requires a policy $\mathbb{P}(\zeta | \mathbf{p})$ that models the design ζ and design constraints [4], along with a sampling procedure to generate $\zeta[k] \sim \mathbb{P}(\zeta[k] | \mathbf{p})$, and the gradient of the log-probability $\nabla_{\mathbf{p}} \log \mathbb{P}(\zeta[k] | \mathbf{p})$ for stochastic optimization.

3. Probabilistic Approach to Optimal Path OED. We formulate the trajectory OED problem as a discrete graph optimization (Problem 3.1), where nodes represent feasible sensor locations and edges encode allowable motion between them.

Problem 3.1: Discrete Path OED Problem on a Graph

Consider a navigation mesh represented by a directed graph $G = (V, E)$, with vertices $V = \{v_1, \dots, v_N\}$, and arcs $E \subseteq V \times V$. The path OED problem seeks a trajectory $\zeta = (\zeta_1, \dots, \zeta_n) \in V^n$ that solves

$$(3.1) \quad \zeta^{\text{opt}} \in \arg \max_{\zeta = (\zeta_1, \dots, \zeta_n) \in V^n} \mathcal{U}(\zeta),$$

where $V^n = V \times \dots \times V$ contains all possible trajectories of length n , and $\mathcal{U}(\zeta)$ is a utility function that quantifies the quality of a path ζ .

Note the following about Problem 3.1. (1) Although related to navigation mesh path planning [13], this framework optimizes path OED objectives rather than shortest paths between prescribed nodes. (2) A directed graph is used to enforce feasible navigation directions, as asymmetric motion constraints substantially increase optimization complexity. (3) Problem 3.1 is abstract and does not prescribe trajectory–model synchronization; when the design specifies an observational path, graph transitions correspond to motion between candidate locations over successive observation times. Path synchronization is application-specific and is addressed in Section 4.

(4) The utility function \mathcal{U} is assumed to be a black box function that can be defined, for example, based on the information gain aggregated over the path.

Standard discrete solution methods for [Problem 3.1](#) are infeasible due to exponential design-space growth, motivating the probabilistic formulation [\(2.2\)](#).

Leveraging [\(2.2\)](#) for path OED, requires a parametric policy $\mathbb{P}(\zeta | \mathbf{p})$ that defines the path probability. We propose three policies in [Subsection 3.1](#). A probabilistic optimization approach that utilizes these policies is then described in [Subsection 3.2](#).

3.1. Probabilistic Policies for the Experimental Path. The experimental path ζ defines the sensor locations at successive time instances. At any time instance t_k , a moving sensor can exist at one and only one location (vertex v_i). The sensor can then move at the next time instance t_{k+1} to a vertex v_j only if there is an edge connecting v_i to v_j , that is, $(v_i, v_j) \in V$. A random trajectory on a graph can be modeled by using a discrete Markov chain (MC) with the general probability model

$$(3.2) \quad \mathbb{P}(\zeta) = \mathbb{P}(\zeta_1, \zeta_2, \dots, \zeta_{n-1}) = \mathbb{P}(\zeta_1)\mathbb{P}(\zeta_2 | \zeta_1)\mathbb{P}(\zeta_3 | \zeta_1, \zeta_2) \dots \mathbb{P}(\zeta_n | \zeta_1 \dots \zeta_{n-1}),$$

where the initial distribution $\mathbb{P}(\zeta_1)$ describes the probability of starting the trajectory at any vertex v_i . The conditional transition probability $\mathbb{P}(\zeta_n | \zeta_1 \dots \zeta_{n-1})$ describes the probability of moving from ζ_{n-1} to ζ_n given the full history $(\zeta_1, \dots, \zeta_{n-1})$.

While a first-order chain assumes that the next location depends only on the current one, high-order chains capture dependencies on multiple previous steps. We first develop a first-order policy based on memoryless MCs in [Subsection 3.1.1](#), then extend the discussion to higher-order MC models in [Subsection 3.1.2](#). An example of the proposed policies is given in the supplementary material (see [Section B](#)).

3.1.1. First-Order Policy. A memoryless MC assumes that the conditional transition probability is given by $\mathbb{P}(\zeta_n | \zeta_{n-1} \dots \zeta_1) = \mathbb{P}(\zeta_n | \zeta_{n-1})$, reducing [\(3.2\)](#) to

$$(3.3) \quad \mathbb{P}(\zeta) = \mathbb{P}(\zeta_1)\mathbb{P}(\zeta_2 | \zeta_1)\mathbb{P}(\zeta_3 | \zeta_2) \dots \mathbb{P}(\zeta_n | \zeta_{n-1}) = \mathbb{P}(\zeta_1) \prod_{t=1}^{n-1} \mathbb{P}(\zeta_{t+1} | \zeta_t).$$

Here $\mathbb{P}(\zeta_{i+1} | \zeta_i)$ describes the probability of moving along the arc (v_i, v_{i+1}) given that the sensor is at v_i . The matrix \mathbf{P} with $[\mathbf{P}]_{ij} = \mathbb{P}(\zeta_{t+1} = v_j | \zeta_t = v_i)$, for any time t and for all $v_i, v_j \in V$, is called the transition probability matrix.

The first-order trajectory distribution [\(3.3\)](#) requires modeling both the initial and the transition distribution. These models are developed next.

Modeling the initial distribution. The initial distribution is given by

$$(3.4) \quad \boldsymbol{\pi} = (\pi_1, \pi_2, \dots, \pi_N); \quad \text{such that} \quad 0 \leq \pi_i \leq 1, \quad \text{and} \quad \sum_{i=1}^N \pi_i = 1,$$

where $\pi_i = \mathbb{P}(\zeta_1 = v_i)$ is the probability that the trajectory starts at $v_i \in V$. Starting at any node can be modeled as a Bernoulli experiment (start at the node or not). Since only one location is allowed, the initial distribution can be defined by employing first-order inclusion probabilities [\[37\]](#). Specifically, assuming that each node v_i is associated with a Bernoulli probability $p_i \in (0, 1)$, the initial distribution is defined as

$$(3.5) \quad \pi_i \equiv \mathbb{P}(\zeta_1 = v_i) = \frac{w_i}{\sum_{j=1}^N w_j}; \quad w_i = \frac{p_i}{1 - p_i}; \quad p_i \in (0, 1), \quad i = 1, 2, \dots, N.$$

The case of degenerate probabilities $\pi_i \in \{0, 1\}$ is omitted for simplicity of the discussion. It can be retrieved, however, by noting that (3.5) is in fact a special case of the conditional Bernoulli model $\mathbb{P}(\mathbf{x} \mid \mathbf{p}, \|\mathbf{x}\|_0 = z)$ with budget $z = 1$, where $\mathbf{x} \in \{0, 1\}^N$ is a binary vector of size N ; see [4] for additional details.

Note that (3.5) inherently models the constraint $\sum_{i=1}^N \pi_i = 1$ and requires only the bound constraints $p_i \in (0, 1)$. We also note that (3.5) is undefined if more than one parameter p_i is equal to 1 or if all parameters p_i are equal to 0. Moreover, the log-probability is undefined when $\pi_i = 0$. These issues do not arise in our framework because sampled policies and gradient optimization maintain the probability-sum constraint. Initial parameters of the optimization procedure can satisfy this, for example, by assuming $p_i = 0.5$ initially, with preferences for certain nodes adjusted as needed.

Modeling the transition distribution. The conditional transition distribution

$$(3.6) \quad \boldsymbol{\pi}^{(i)} = (\pi_1^i, \dots, \pi_N^i); \quad \sum_{i=1}^N \pi_j^i = 1, \quad 0 \leq \pi_j^i \leq 1, \quad \pi_j^i = 0 \text{ for } (v_i, v_j) \notin V,$$

defines $\pi_j^i = \mathbb{P}(v_j \mid v_i) \equiv \mathbb{P}(\zeta_{t+1} = v_j \mid \zeta_t = v_i)$, the probability of moving in one step from v_i to v_j . Assuming a stationary chain, the transition probability π_j^i is independent of time or the position of (v_i, v_j) in the trajectory.

The transition distribution (3.6) can be modeled by following the same approach employed for modeling the initial distribution. Specifically, we associate with each vertex v_i a vector of Bernoulli probabilities—modeling the possibility of either to transition or not—of moving to another node v_j . Since moving to a node v_j such that $(v_i, v_j) \notin V$ has to be zero, we need to model only the probability of moving to a node v_j in the neighborhood $\mathcal{N}(v_i)$ of v_i . Specifically, by letting

$$(3.7) \quad \mathbf{p}^{(i)} = (p_1^i, \dots, p_{N_i}^i); \quad 0 \leq p_j^i \leq 1 \forall v_j \in \mathcal{N}(v_i), \quad p_j^i = 0 \forall v_j \notin \mathcal{N}(v_i),$$

the transition probabilities associated with node v_i are defined as

$$(3.8) \quad \pi_j^i = \mathbb{P}(\zeta_{t+1} = v_j \mid \zeta_t = v_i) = \frac{w_j^i}{\sum_{j=1}^{N_i} w_j^i}; \quad w_j^i = \frac{p_j^i}{1 - p_j^i}; \quad p_j^i \in (0, 1).$$

Note that p_i is the probability of starting from v_i irrespective of the other nodes. Conversely, π_i is the probability that a trajectory exclusively starts at v_i . Similarly, given that the sensor is at v_i , π_j^i is the probability of moving exclusively to v_j . These distinctions reflect that a sensor can occupy or move to only one node at a time.

Definition 3.1 formalizes the proposed first-order path policy.

Definition 3.1: First-Order Path Policy

The probability distribution of a path $\zeta = (\zeta_1, \zeta_2, \dots, \zeta_n)$ of fixed size n , parametrized by the parameter $\mathbf{p} \in (0, 1)^{N(N+1)}$, is given by

$$(3.9a) \quad \mathbb{P}(\zeta) = \mathbb{P}(\zeta_1) \prod_{t=1}^{n-1} \mathbb{P}(\zeta_{t+1} \mid \zeta_t),$$

$$(3.9b) \quad \mathbf{p} = \left(\underbrace{p_1, \dots, p_N}_{\text{initial parameters}} ; \underbrace{p_1^1, \dots, p_N^1; \dots; p_1^N, \dots, p_N^N}_{\text{transition parameters}} \right),$$

$$(3.9c) \quad \mathbb{P}(\zeta_1 = v_i) = \pi_i = \frac{w_i}{\sum_{j=1}^N w_j}; \quad w_i = \frac{p_i}{1-p_i}, \quad i = 1, \dots, N,$$

$$(3.9d) \quad \mathbb{P}(\zeta_{t+1} = v_j \mid \zeta_t = v_i) = \pi_j^i = \frac{w_j^i}{\sum_{k=1}^N w_k^i}; \quad w_j^i = \frac{p_j^i}{1-p_j^i}, \quad i = 1, \dots, N, \quad j = 1, \dots, N.$$

Although [Definition 3.1](#) defines $\mathbf{p} \in (0, 1)^{N^2+N}$, in practice the effective parameter space is much smaller since each node connects only to a few neighbors. Thus, one needs to store only the nonzero parameters, reducing the parameter space to $N(C+1)$, where C is the maximum neighborhood cardinality.

The gradient of the log-probability $\nabla_{\mathbf{p}} \log(\mathbb{P}(\zeta))$ is required for the probabilistic optimization approach and is summarized by [Proposition 3.1](#).

PROPOSITION 3.1. *The policy (3.9) has the following gradient of log-probability:*

$$(3.10a) \quad \nabla_{\mathbf{p}} \log(\mathbb{P}(\zeta)) = \nabla_{\mathbf{p}} \log(\mathbb{P}(\zeta_1)) + \sum_{i=1}^{n-1} \nabla_{\mathbf{p}} \log(\mathbb{P}(\zeta_{i+1} \mid \zeta_i)),$$

with elementwise components of the gradient vector given by

$$(3.10b) \quad \frac{\partial \log \pi_i}{\partial p_j} = \frac{\partial \log \mathbb{P}(\zeta_1 = v_i)}{\partial p_j} = \frac{1}{(1-p_j)^2} \left(\frac{\delta_{ij}}{w_j} - \frac{1}{\sum_{k=1}^N w_k} \right),$$

$$(3.10c) \quad \frac{\partial \log \pi_j^i}{\partial p_m^l} = \frac{\partial \log \mathbb{P}(\zeta_{t+1} = v_j \mid \zeta_t = v_i)}{\partial p_m^l} = \frac{\delta_{il}}{(1-p_m^l)^2} \left(\frac{\delta_{jm}}{w_m^l} - \frac{1}{\sum_{k=1}^N w_k^l} \right),$$

where δ_{ij} is the Kronecker delta function with $\delta_{ij} = 1$ when $i = j$ and 0 otherwise.

Proof. See [Section A](#). □

The first-order policy is memoryless, assuming the next node depends only on the current one. Trajectories may benefit from memory, which can be captured by using higher-order Markov chains [[15](#), Chapter 6] as discussed in the following subsection.

3.1.2. Higher-Order Path Policies. The k th-order MC satisfies

$$(3.11) \quad \mathbb{P}(\zeta_n \mid \zeta_1, \zeta_2, \dots, \zeta_{n-2}, \zeta_{n-1}) = \mathbb{P}(\zeta_n \mid \zeta_{n-k}, \zeta_{n-k+1}, \dots, \zeta_{n-2}, \zeta_{n-1}), \quad k \in \mathbb{Z}^+,$$

where the case of $k = 1$ reduces to the first-order (memoryless) MC (3.3).

Standard higher-order MC is rarely used in practice because the size of the transition tensor (3.11) is $\mathcal{O}(N^k)$, which grows exponentially with the order k . Practical approaches, such as the Raftery model [34], extend a first-order model by introducing a single additional parameter for each lag:

$$(3.12) \quad \mathbb{P}(\zeta_n | \zeta_{n-k}, \zeta_{n-k+1}, \dots, \zeta_{n-2}, \zeta_{n-1}) = \sum_{i=1}^k \lambda_i \mathbb{P}(\zeta_n | \zeta_{n-i}); \quad \sum_{i=1}^k \lambda_i = 1,$$

where $\mathbb{P}(\zeta_n | \zeta_{n-i})$ is the one-step transition probability (3.8). This is similar to the first-order autoregressive model, where a linear combination is taken over subsequent lags. A generalization of (3.12) was developed in [14] to allow the transition probability $\mathbb{P}(\zeta_n | \zeta_{n-i})$ to be different for each lag, affording more flexibility.

In the remainder of [Subsection 3.1.2](#) we develop two probabilistic policies for the trajectory based on the Raftery model and its generalization.

Path policy based on the Raftery model. Here the path probability (3.2) is

$$(3.13) \quad \begin{aligned} \mathbb{P}(\zeta) &= \mathbb{P}(\zeta_1, \dots, \zeta_n) = \mathbb{P}(\zeta_n | \zeta_1, \dots, \zeta_{n-1}) \mathbb{P}(\zeta_1, \dots, \zeta_{n-1}) \\ &= \mathbb{P}(\zeta_1, \zeta_2, \dots, \zeta_k) \prod_{t=k}^{n-1} \mathbb{P}(\zeta_{t+1} | \zeta_{t-k+1}, \dots, \zeta_{t-1}, \zeta_t), \end{aligned}$$

where the conditional probability rule is applied repeatedly, and (3.11) is used to obtain (3.13). We employ the first-order policy to model the initial distribution (over k steps) $\mathbb{P}(\zeta_1, \dots, \zeta_k)$. The parameters \mathbf{p} of this model would be the same as (3.9b) in addition to the lag parameters $\lambda_1, \dots, \lambda_k$ as formalized by [Definition 3.2](#).

Definition 3.2: Higher-Order Path Policy

For a positive integer $k \in \mathbb{Z}^+$, the k th-order probability distribution of a path $\zeta = (\zeta_1, \dots, \zeta_n)$ of fixed size $n > k$, parametrized by $\mathbf{p} \in (0, 1)^{N(N+1)+k}$, is

$$(3.14a) \quad \mathbb{P}(\zeta) = \mathbb{P}(\zeta_1) \prod_{t=1}^{k-1} (\mathbb{P}(\zeta_{t+1} | \zeta_t)) \prod_{t=k}^{n-1} \left(\sum_{i=1}^k \lambda_i \mathbb{P}(\zeta_{t+1} | \zeta_{t+1-i}) \right),$$

$$(3.14b) \quad \mathbf{p} = (p_1, \dots, p_N; p_1^1, \dots, p_N^1, \dots, p_1^N, \dots, p_N^N; \lambda_1, \dots, \lambda_k); \quad \sum_{i=1}^k \lambda_i = 1,$$

$$(3.14c) \quad \mathbb{P}(\zeta_1 = v_i) = \pi_i = \frac{w_i}{\sum_{j=1}^N w_j}; \quad w_i = \frac{p_i}{1 - p_i}, \quad i = 1, \dots, N,$$

$$(3.14d) \quad \mathbb{P}(v_j | v_i) = \pi_j^i = \frac{w_j^i}{\sum_{k=1}^N w_k^i}; \quad w_j^i = \frac{p_j^i}{1 - p_j^i}, \quad i = 1, \dots, N, \quad j = 1, \dots, N,$$

where $\mathbb{P}(\zeta_{t+z} = v_j | \zeta_t = v_i) = \pi_j^i$ for any positive integer z .

PROPOSITION 3.2. *The gradient of the log-policy given by (3.14) is given by*

$$(3.15a) \quad \left(\frac{\partial}{\partial p_1}, \dots, \frac{\partial}{\partial p_N}; \frac{\partial}{\partial p_1^1}, \dots, \frac{\partial}{\partial p_N^1}; \dots; \frac{\partial}{\partial p_1^N}, \dots, \frac{\partial}{\partial p_N^N}; \frac{\partial}{\partial \lambda_1}, \dots, \frac{\partial}{\partial \lambda_k} \right) \log \mathbb{P}(\zeta),$$

with elementwise components given as follows:

$$(3.15b) \quad \frac{\partial \log \mathbb{P}(\zeta)}{\partial p_j} = \frac{\partial \log \mathbb{P}(\zeta_1)}{\partial p_j},$$

$$(3.15c) \quad \frac{\partial \log \mathbb{P}(\zeta)}{\partial p_m^l} = \sum_{t=1}^{k-1} \frac{\partial \log \mathbb{P}(\zeta_{t+1} | \zeta_t)}{\partial p_m^l} + \sum_{t=k}^{n-1} \frac{\sum_{i=1}^k \lambda_i \frac{\partial \mathbb{P}(\zeta_{t+1} | \zeta_{t+1-i})}{\partial p_m^l}}{\sum_{i=1}^k \lambda_i \mathbb{P}(\zeta_{t+1} | \zeta_{t+1-i})}$$

$$(3.15d) \quad \frac{\partial \log \mathbb{P}(\zeta)}{\partial \lambda_l} = \sum_{t=k}^{n-1} \frac{\mathbb{P}(\zeta_{t+1} | \zeta_{t+1-l})}{\sum_{i=1}^k \lambda_i \mathbb{P}(\zeta_{t+1} | \zeta_{t+1-i})},$$

where $\frac{\partial \log \mathbb{P}(\zeta_1 = v_i)}{\partial p_j} = \frac{\partial \log \pi_i}{\partial p_j}$ is given by (3.10b); $\frac{\partial \log \mathbb{P}(\zeta_{t+z} = v_j | \zeta_t = v_i)}{\partial p_m^l} = \frac{\partial \log \pi_j^i}{\partial p_m^l}$ is given by (3.10c) for any positive integer z ; and $\frac{\partial \pi_j^i}{\partial p_m^l} = \pi_j^i \frac{\partial \log \pi_j^i}{\partial p_m^l}$.

Proof. See Section A. □

Path policy based on a generalized Raftery model. The original Raftery model (3.12) freezes the transition probabilities for all lags. Specifically, as described by (3.14d), the transition probabilities are given by $\mathbb{P}(\zeta_* = v_j | \zeta_* = v_i)$ irrespective of the lag, that is, irrespective of the order of the states ζ_* in the trajectory or with respect to each other. This approach can be restrictive, however, especially since in our application connectivity of the navigation mesh is sparse. Thus, for a given vertex the memory is mostly restricted to neighboring cells. Moreover, the time-dependent nature of predictive applications might not be sufficiently captured by this model. An alternative approach is to employ the lag-dependent conditional probability:

$$(3.16) \quad \mathbb{P}(\zeta_n | \zeta_{n-k}, \dots, \zeta_{n-2}, \zeta_{n-1}) = \sum_{i=1}^k \lambda_i \mathbb{P}^{(i)}(\zeta_n | \zeta_{n-i}); \quad \sum_{i=1}^k \lambda_i = 1,$$

where for each lag $l = 1, \dots, k$, the conditional transition probabilities form a matrix $\mathbf{P}^{(l)}$ with $[\mathbf{P}^{(l)}]_{ij} = \{\mathbb{P}^{(l)}(\zeta_{t+1} = v_j | \zeta_t = v_i)\}$ that satisfies the conditions of a probability transition matrix; that is, the entries fall within $[0, 1]$, and each row adds to 1. As suggested in [14, 16], we define $\mathbf{P}^{(l)} = \prod_{i=1}^l \mathbf{P}$ for $l = 1, \dots, k$, where $\mathbf{P} = \mathbf{P}^{(1)}$ is the first-order transition probability matrix used in the original Raftery model (3.12).

Note that this generalization does not change the number of parameters in the model since all transition probabilities depend on the first-order transition probability. The proposed path distribution is summarized by Definition 3.3.

Definition 3.3: Generalized Higher-Order Path Policy

For $k \in \mathbb{Z}^+$, the generalized k th-order probability distribution of a path $\zeta = (\zeta_1, \dots, \zeta_n)$ of fixed size $n > k$, parametrized by $\mathbf{p} \in (0, 1)^{N(N+1)+k}$, is

$$(3.17a) \quad \mathbb{P}(\zeta) = \mathbb{P}(\zeta_1) \prod_{t=1}^{k-1} (\mathbb{P}(\zeta_{t+1} | \zeta_t)) \prod_{t=k}^{n-1} \left(\sum_{i=1}^k \lambda_i \mathbb{P}^{(i)}(\zeta_{t+1} | \zeta_{t+1-i}) \right),$$

$$(3.17b) \quad \mathbf{p} = (p_1, \dots, p_N; p_1^1, \dots, p_N^1, \dots, p_1^N, \dots, p_N^N; \lambda_1, \dots, \lambda_k); \quad \sum_{i=1}^k \lambda_i = 1,$$

$$(3.17c) \quad \mathbb{P}(\zeta_1 = v_i) \equiv \pi_i = \frac{w_i}{\sum_{j=1}^N w_j}; \quad w_i = \frac{p_i}{1-p_i},$$

$$(3.17d) \quad \mathbb{P}(\zeta_{t+1} = v_j \mid \zeta_t = v_i) \equiv \pi_j^i = \frac{w_j^i}{\sum_{k=1}^N w_k^i}; \quad w_j^i = \frac{p_j^i}{1-p_j^i},$$

$$(3.17e) \quad \mathbb{P}^{(r)}(\zeta_t = v_j \mid \zeta_{t-r} = v_i) = \sum_{k_{r-1}=1}^N \cdots \sum_{k_2=1}^N \sum_{k_1=1}^N \pi_{k_{r-1}}^i \pi_{k_{r-2}}^{k_{r-1}} \cdots \pi_{k_1}^{k_2} \pi_{k_j}^{k_1}.$$

While the r summations in (3.17e) are written over N possible states, in our application most of the terms vanish because of lack of connectivity in the navigation mesh. Each summation reduces to the number of connected nodes (via a path of length up to the predefined policy order k) to a given node.

PROPOSITION 3.3. *The gradient of the log-policy in (3.17) is given by*

$$(3.18a) \quad \left(\frac{\partial}{\partial p_1}, \dots, \frac{\partial}{\partial p_N}; \frac{\partial}{\partial p_1^1}, \dots, \frac{\partial}{\partial p_N^1}; \dots; \frac{\partial}{\partial p_1^N}, \dots, \frac{\partial}{\partial p_N^N}; \frac{\partial}{\partial \lambda_1}, \dots, \frac{\partial}{\partial \lambda_k} \right) \log \mathbb{P}(\zeta),$$

with elementwise components given as follows:

$$(3.18b) \quad \frac{\partial \log \mathbb{P}(\zeta)}{\partial p_j} = \frac{\partial \log \mathbb{P}(\zeta_1)}{\partial p_j},$$

$$(3.18c) \quad \frac{\partial \log \mathbb{P}(\zeta)}{\partial p_m^l} = \sum_{t=1}^{k-1} \frac{\partial \log \mathbb{P}(\zeta_{t+1} \mid \zeta_t)}{\partial p_m^l} + \sum_{t=k}^{n-1} \frac{\sum_{i=1}^k \lambda_i \frac{\partial \mathbb{P}^{(i)}(\zeta_{t+1} \mid \zeta_{t+1-i})}{\partial p_m^l}}{\sum_{i=1}^k \lambda_i \mathbb{P}^{(i)}(\zeta_{t+1} \mid \zeta_{t+1-i})},$$

$$(3.18d) \quad \frac{\partial \log \mathbb{P}(\zeta)}{\partial \lambda_l} = \sum_{t=k}^{n-1} \frac{\mathbb{P}^{(l)}(\zeta_{t+1} \mid \zeta_{t+1-l})}{\sum_{i=1}^k \lambda_i \mathbb{P}^{(i)}(\zeta_{t+1} \mid \zeta_{t+1-i})},$$

$$(3.18e) \quad \frac{\partial \mathbb{P}^{(r)}(\zeta_t = v_j \mid \zeta_{t-r} = v_i)}{\partial p_m^l} = \sum_{k_{r-1}=1}^N \cdots \sum_{k_2=1}^N \sum_{k_1=1}^N \frac{\partial \left(\pi_{k_{r-1}}^i \pi_{k_{r-2}}^{k_{r-1}} \cdots \pi_{k_1}^{k_2} \pi_{k_j}^{k_1} \right)}{\partial p_m^l},$$

where $\frac{\partial \log \pi_i}{\partial p_j}$ is given by (3.10b) and $\frac{\partial \log \pi_j^i}{\partial p_m^l}$ is given by (3.10c).

Proof. See Section A. □

3.1.3. Fixing the Lag Weights. The lag weights control how past steps influence the next move. They can be fixed and excluded from the policy parameters as their gradients vanish. For example, $\lambda_i = \frac{1}{k}$ enforces uniform influence. Stronger influence from more recent steps can be achieved, for example, by setting $\lambda_i = \gamma^{i-1}$ with a discount factor $0 < \gamma \leq 1$, as followed in policy optimization methods [12].

In Definition 3.2 the conditional probability $\mathbb{P}(\zeta_n \mid \zeta_{n-k}, \zeta_{n-k+1}, \dots, \zeta_{n-2}, \zeta_{n-1})$ is nonzero when the transition probability $\mathbb{P}(\zeta_n \mid \zeta_{n-i})$ from any node in the past, up to the defined order $\zeta_{n-i}, i = 1, \dots, k$, is nonzero. Similarly, Definition 3.3 assigns nonzero values for the conditional transition probability when there is a path of length i between ζ_{n-i} and ζ_n for any $i \leq k$. This means that these models can allow trajectories involving jumps between nodes without direct arcs connecting them. This

effect is expected to magnify with longer trajectories and/or higher orders, as shown in the numerical results in [Section 4](#). Thus, we recommend modeling the lag parameters with a decaying sequence of fixed values. For example, to avoid tuning a discount factor, in [Section 4](#) we consider the following normalized geometric model:

$$(3.19) \quad \lambda_i = \frac{\frac{1}{i}}{\sum_{i=1}^k \frac{1}{i}}, \quad i = 1, 2, \dots, k.$$

3.1.4. Sampling Trajectories. Sampling trajectories from the parametric policy is critical for the the probabilistic optimization approach. Sampling trajectories from first-order policy ([Definition 3.1](#)) is described by [Algorithm 3.1](#), and sampling the higher-order policies ([Definition 3.2](#), [Definition 3.3](#)) is described by [Algorithm 3.2](#).

Algorithm 3.1 Sample trajectories from first-order policy model ([Definition 3.1](#)).

Input: Distribution parameters \mathbf{p} ([3.9b](#)); trajectory length n ; and sample size N_{ens} .
Output: A sample $\{\zeta[i] \in V^n \sim \mathbb{P}(\zeta | \mathbf{p}) | i = 1, \dots, N_{\text{ens}}\}$ drawn from ([3.9a](#))

- 1: Initialize a sample $S = \{\}$.
- 2: **for** $i \leftarrow 1$ to N_{ens} **do**
- 3: Extract initial parameters (p_1, \dots, p_N) from \mathbf{p}
- 4: Compute initial inclusion probabilities (π_1, \dots, π_N) ▷ Use ([3.9c](#))
- 5: Sample initial vertex $\zeta_1[i] \in V$ with probabilities $\mathbb{P}(v_i) = \pi_i$, $i = 1, \dots, N$
- 6: **for** $j \leftarrow 2$ to n **do**
- 7: Extract transition parameters (p_1^z, \dots, p_N^z) from \mathbf{p} with $\zeta_{j-1}[i] = v_z \in V$
- 8: Compute transition probabilities π_1^z, \dots, π_N^z ▷ Use ([3.9d](#))
- 9: Sample next vertex $\zeta_j[i] \in V$ with probabilities $\mathbb{P}(v_i) = \pi_i^z$, $i = 1, \dots, N$
- 10: **end for**
- 11: Update $S \leftarrow S \cup \{\zeta[i]\}$
- 12: **end for**
- 13: **return** S

Algorithm 3.2 Sample higher-order policy models [Definition 3.2](#) (or [Definition 3.3](#)).

Input: Policy order $k > 1$, parameters \mathbf{p} ([3.14b](#)) (or ([3.17b](#))); trajectory length $n > k$; and sample size N_{ens} .
Output: Sample $\{\zeta[i] \in V^n \sim \mathbb{P}(\zeta | \mathbf{p}) | i = 1, \dots, N_{\text{ens}}\}$ from ([3.14a](#)) (or ([3.17a](#))).

- 1: Initialize a sample $S = \{\}$.
- 2: **for** $i \leftarrow 1$ to N_{ens} **do**
- 3: Sample initial k nodes $(\zeta_1[i], \dots, \zeta_k[i])$ of the path ▷ Use [Algorithm 3.1](#)
- 4: **for** $j \leftarrow k + 1$ to n **do**
- 5: Extract transition parameters (p_1^z, \dots, p_N^z) from \mathbf{p} with $\zeta_{j-1}[i] = v_z \in V$
- 6: Compute transition probabilities π_1^z, \dots, π_N^z ▷ Use ([3.14d](#)) (or ([3.17d](#)))
- 7: Sample next vertex $\zeta_j[i] \in V$ with probabilities $\mathbb{P}(v_i) = \pi_i^z$, $i = 1, \dots, N$
- 8: **end for**
- 9: Update $S \leftarrow S \cup \{\zeta[i]\}$
- 10: **end for**
- 11: **return** S

In Step 6 of [Algorithm 3.1](#) transitions need to be evaluated only over the local neighborhood of the current node, reducing the sampling computational cost. In

contrast, sampling the higher-order policies (Step 4 of [Algorithm 3.2](#)) involves linear combinations of transitions up to order k , requiring an extended neighborhood that can be precomputed offline based on graph connectivity and the model order.

3.2. Probabilistic Path OED Problem. We replace the discrete path OED Problem 3.1 with the probabilistic formulation given by [Problem 3.2](#).

Problem 3.2: Probabilistic Path OED Problem on a Graph

Given the setup in [Problem 3.1](#), the probabilistic path OED problem is

$$(3.20) \quad \mathbf{p}^{\text{opt}} \in \arg \max_{\zeta \sim \mathbb{P}(\zeta | \mathbf{p})} \mathbb{E}_{\zeta \sim \mathbb{P}(\zeta | \mathbf{p})} [\mathcal{U}(\zeta)],$$

where $\mathbb{P}(\zeta | \mathbf{p})$ is given by [Definition 3.1](#), [Definition 3.2](#), or [Definition 3.3](#).

We numerically solve (3.20) using the stochastic gradient $\hat{\mathbf{g}}$ given by (2.3). At each iteration, the parameters are updated by projected stochastic gradient ascent (or descent for minimization), with a prescribed step size, ensuring feasibility by projecting onto $[0, 1]^{N_p}$. The update step of the policy parameter is thus given by

$$(3.21) \quad \mathbf{p}^{(n)} \leftarrow P(\mathbf{p}^{(n-1)} + \eta^{(n)} \hat{\mathbf{g}}),$$

where $0 < \eta^{(n)} \leq 1$ is a positive step size (learning rate) at the n th iteration of the optimization procedure and the plus sign in (3.21) is replaced with a minus sign for minimization (steepest descent). As proposed in [4], we employ the scaling projector:

$$(3.22) \quad P(\mathbf{g}) = s \mathbf{g}; \quad s = \min\{1, \min_{i=1, \dots, N_p} \{s_i\}\}; \quad s_i = \begin{cases} \frac{1-p_i}{|g_i|} & \text{if } p_i \pm g_i > 1 \\ \frac{p_i}{|g_i|} & \text{if } p_i \pm g_i < 0 \\ 1 & \text{otherwise,} \end{cases}$$

which restricts (by scaling) the updated parameter $\mathbf{g} \pm \mathbf{p}$ to the domain $[0, 1]^N$ and \pm defines the projected gradient for both maximization and minimization, respectively. When the higher-order models are employed, the lag weights are normalized $\lambda_i \leftarrow \lambda_i / \sum_{i=1}^k \lambda_i$ after applying the projection operator.

With limited sample sizes N_{ens} due to expensive utility function evaluations, stochastic gradient variance can be high, leading to unstable learning. This is mitigated by introducing a constant baseline function b to (3.20) by replacing \mathcal{U} with $\mathcal{U} - b$. This does not alter the optimal solution since $\arg \max_{\zeta \sim \mathbb{P}(\zeta | \mathbf{p})} \mathbb{E}_{\zeta \sim \mathbb{P}(\zeta | \mathbf{p})} [\mathcal{U}(\zeta)] = \arg \max_{\zeta \sim \mathbb{P}(\zeta | \mathbf{p})} \mathbb{E}_{\zeta \sim \mathbb{P}(\zeta | \mathbf{p})} [\mathcal{U}(\zeta) - b] = \arg \max_{\zeta \sim \mathbb{P}(\zeta | \mathbf{p})} \mathbb{E}_{\zeta \sim \mathbb{P}(\zeta | \mathbf{p})} [\mathcal{U}(\zeta)] - b$. Moreover, the gradient satisfies $\mathbf{g}^b = \nabla_{\mathbf{p}} \mathbb{E}_{\zeta \sim \mathbb{P}(\zeta | \mathbf{p})} [\mathcal{U}(\zeta) - b] = \nabla_{\mathbf{p}} \mathbb{E}_{\zeta \sim \mathbb{P}(\zeta | \mathbf{p})} [\mathcal{U}(\zeta)] = \mathbf{g}$. The stochastic estimate of the gradient, however, becomes

$$(3.23a) \quad \hat{\mathbf{g}}^b = \frac{1}{N_{\text{ens}}} \sum_{k=1}^{N_{\text{ens}}} \mathcal{U}(\zeta[k] - b) \nabla_{\mathbf{p}} \log \mathbb{P}(\zeta[k] | \mathbf{p}); \quad \zeta[k] \sim \mathbb{P}(\zeta | \mathbf{p}).$$

Both (2.3b) and (3.23a) are unbiased estimators of \mathbf{g} (2.3a). By letting

$$(3.23b) \quad \mathbf{d} = \frac{1}{N_{\text{ens}}} \sum_{k=1}^{N_{\text{ens}}} \nabla_{\mathbf{p}} \log \mathbb{P}(\zeta[k] | \mathbf{p}); \quad \zeta[k] \sim \mathbb{P}(\zeta | \mathbf{p}),$$

we note that $\hat{\mathbf{g}}^b = \hat{\mathbf{g}} - b \mathbf{d}$, and thus $\mathbb{E}[\hat{\mathbf{g}}] = \mathbb{E}[\hat{\mathbf{g}}^b] = \mathbf{g}$, where we used the fact that $\mathbb{E}[\mathbf{d}] = \mathbf{0}$. Moreover, the total variance of the two stochastic estimators is such that $\text{var}(\hat{\mathbf{g}}^b) = \text{var}(\hat{\mathbf{g}}) - 2b\mathbb{E}[\hat{\mathbf{g}}^\top \mathbf{d}] + b^2\mathbb{E}[\mathbf{d}^\top \mathbf{d}]$, which is a quadratic in the baseline b . The value of the baseline that minimizes the variance $\text{var}(\hat{\mathbf{g}}^b)$ is thus

$$(3.23c) \quad b^{\text{opt}} = (\mathbb{E}[\hat{\mathbf{g}}^\top \mathbf{d}]) / (\mathbb{E}[\hat{\mathbf{d}}^\top \mathbf{d}]).$$

The optimal baseline (3.23c) applies to any parametric policy $\mathbb{P}(\zeta | p)$ and has a denominator that depends only on the policy, allowing closed-form evaluation, while the numerator depends on the utility and is generally intractable analytically. Because of correlations and combinatorial complexity, (3.23c) is efficiently estimated by

$$(3.23d) \quad \begin{aligned} b^{\text{opt}} &\approx \frac{\sum_{i=1}^{N_b} (\hat{\mathbf{g}}[i])^\top \mathbf{d}[i]}{\sum_{i=1}^{N_b} (\mathbf{d}[i])^\top \mathbf{d}[i]}, \\ \mathbf{d}[i] &= \frac{\sum_{j=1}^{N_{\text{ens}}} \nabla_{\mathbf{p}} \log \mathbb{P}(\zeta[i, j])}{N_{\text{ens}}}; \quad \hat{\mathbf{g}}[i] = \frac{\sum_{j=1}^{N_{\text{ens}}} \mathcal{U}(\zeta[i, j]) \nabla_{\mathbf{p}} \log \mathbb{P}(\zeta[i, j])}{N_{\text{ens}}}, \end{aligned}$$

where $\{\zeta[i, j] \sim \mathbb{P}(\zeta | \mathbf{p}) \mid i = 1, \dots, N_b, j = 1, \dots, N_{\text{ens}}\}$.

3.2.1. Complete Algorithmic Statement. Algorithm 3.3 provides a complete algorithmic statement of the proposed probabilistic path optimization approach.

Algorithm 3.3 Probabilistic Path OED Optimization Algorithm for Solving (3.2).

Input: Utility function \mathcal{U} ; probabilistic policy (either (3.9), (3.14), or (3.17)); initial distribution parameter $\mathbf{p}^{(0)}$; stepsize schedule $\eta^{(n)}$; sample sizes $N_{\text{ens}}, N_{\text{opt}}$.

Output: ζ^{opt}

- 1: initialize $n = 0$
- 2: **while** Not Converged **do**
- 3: Sample $\{\zeta[k]; k = 1, \dots, N_{\text{ens}}\}$ \triangleright Algorithm 3.1 for (3.9)
Algorithm 3.2 for (3.14) or (3.17)
- 4: Evaluate $\{\mathcal{U}(\zeta[k]); k = 1, \dots, N_{\text{ens}}\}$
- 5: Evaluate $\{\nabla_{\mathbf{p}} \log \mathbb{P}(\zeta[k] | \mathbf{p}) ; k = 1, \dots, N_{\text{ens}}\}$ \triangleright Based on the chosen policy
- 6: Calculate $\hat{\mathbf{g}}^{(n)} \leftarrow \frac{1}{N_{\text{ens}}} \sum_{k=1}^{N_{\text{ens}}} \mathcal{U}(\zeta[k]) \nabla_{\mathbf{p}} \log \mathbb{P}(\zeta[k] | \mathbf{p})$
- 7: Calculate $\mathbf{d} \leftarrow \frac{1}{N_{\text{ens}}} \sum_{k=1}^{N_{\text{ens}}} \nabla_{\mathbf{p}} \log \mathbb{P}(\zeta[k] | \mathbf{p})$ \triangleright Use (3.23b)
- 8: Calculate $b \leftarrow \frac{(\hat{\mathbf{g}}^{(n)})^\top \mathbf{d}}{\mathbf{d}^\top \mathbf{d}}$ \triangleright Use (3.23d) with $N_b > 1$ if needed
- 9: Update $\mathbf{p}^{(n+1)} = \mathbf{p}^{(n)} + \eta^{(n)} P(\hat{\mathbf{g}}^{(n)} - b\mathbf{d})$ \triangleright Use P given by (3.22)
- 10: Update $n \leftarrow n + 1$
- 11: **end while**
- 12: Set $\mathbf{p}^{\text{opt}} = \mathbf{p}^{(n)}$
- 13: Sample $\{\zeta[k]; k = 1, \dots, N_{\text{opt}}\}$ with the optimal parameter \mathbf{p}^{opt} .
- 14: **return** ζ^{opt} : the design with largest \mathcal{U} value in the sample.

Algorithm 3.3 is presented for maximization; minimization is handled by flipping the parameter update sign in Step 9, and the optimum design ζ^{opt} in Step 14 is the one with smallest \mathcal{U} value. For simplicity, the baseline is estimated (Step 8) by using the same samples as the stochastic gradient, which is validated in Section 4, although

larger batch sizes may be used. Termination is ensured by standard stopping criteria, such as iteration limits or projected-gradient tolerances, as discussed in Section 4.

Convergence of the algorithm. By design, the proposed approach enjoys all properties of the probabilistic optimization approach for black-box binary optimization presented, for example, in [4, 8]. Convergence is thus guaranteed in expectation, and the set of optimal solutions of the original optimization problem is guaranteed to be a subset of the optimal set of parameters of the probabilistic formulation. The output of Algorithm 3.3 is thus expected to explore the upper tail of the distribution of the utility function \mathcal{U} ; however, global optimality is not generally guaranteed.

3.2.2. Computational Considerations and Scalability. The probabilistic approach requires only utility evaluations, making it independent of the OED criterion and well suited for graph-based path optimization with black-box objectives. Its only requirement is a discrete navigation mesh of the domain. Here we analyze computational bottlenecks, scalability, parallelization opportunities, and limitations of Algorithm 3.3. Discussion of policy selection is deferred to Section 5.

Each iteration of Algorithm 3.3 is dominated by policy sampling (Step 3), utility \mathcal{U} evaluation (Step 4), and log-probability gradients (Step 5). Since \mathcal{U} is treated as a black box, acceleration techniques such as randomization or surrogates apply but are beyond this work; we therefore focus on the costs of sampling and gradient evaluation.

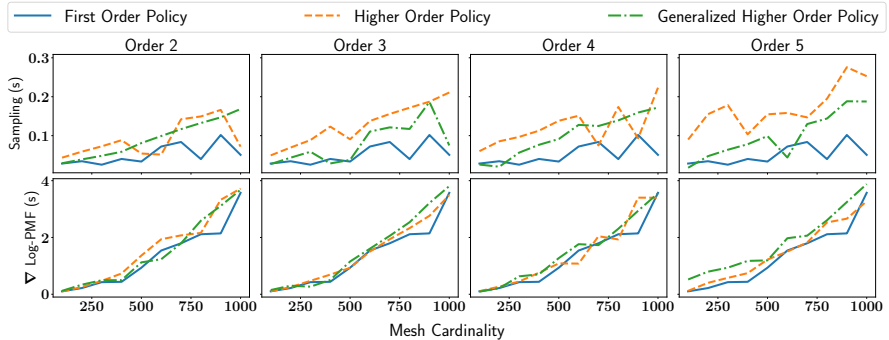


Fig. 1: Wall times against mesh cardinality (number of nodes) for sampling (top) and log-policy gradient (bottom) across the three policy models, averaged over 32 runs on an Apple M1 Mac laptop without parallelization. First-order, higher-order, and generalized higher-order models correspond to Definition 3.1, Definition 3.2, and Definition 3.3, respectively. Results of the first-order policy are repeated for comparison.

Figure 1 reports average wall times for sampling and log-policy gradient across the three policy models. Gradient evaluation (bottom row) is more expensive than sampling (top row), and the higher-order policy incurs the highest sampling cost due to transitions to all reachable nodes, whereas the first-order and the generalized higher-order policies restrict transitions to local or precomputed neighborhoods, reducing cost. Additionally, log-policy gradient scales almost linearly for the three proposed models. This applies to the first two policies. For the third, gradient evaluation requires derivatives of higher-order transitions (3.17e), involving all paths up to order k between nodes. Since the mesh is static and k is fixed, these paths can be precomputed, and automatic differentiation can further aid scalability.

Beyond utility evaluation, gradient computation can benefit the most from paral-

lization. Stochastic gradients can be distributed across samples, and for each sample log-probability gradients can be computed in parallel over path elements. This approach is straightforward for the first two policies but requires extra care for the higher-order model due to derivative evaluation of higher-order transitions.

4. Numerical Experiments. We numerically test the proposed approach using an advection-diffusion simulation common in OED [6, 31], presenting results from multiple experiments, all conducted within the PyOED framework [18].

4.1. Experimental Setup. The advection-diffusion model simulates the spatiotemporal evolution of a contaminant field $u = u(\mathbf{x}, t)$ in a closed domain \mathcal{D} . Given a navigation mesh, we seek an optimal path for moving sensors to measure u .

Model setup: advection-diffusion. The contaminant field u is governed by

$$(4.1) \quad \begin{aligned} u_t - \kappa \Delta u + \mathbf{v} \cdot \nabla u &= 0 & \text{in } \mathcal{D} \times [0, T], \\ u(x, 0) &= \theta & \text{in } \mathcal{D}, \\ \kappa \nabla u \cdot \mathbf{n} &= 0 & \text{on } \partial\mathcal{D} \times [0, T], \end{aligned}$$

where $\kappa > 0$ is the diffusivity and T is the simulation final time. The spatial domain is $\mathcal{D} = [0, 1]^2$ with two rectangular interior regions representing buildings where flow cannot enter. The boundary $\partial\mathcal{D}$ includes both the outer boundary and the building walls. Here \mathbf{v} is the velocity (Figure 2, left) that is obtained by solving a steady Navier–Stokes equation with sidewall–driven flow. The initial contaminant distribution shown in Figure 2 is used as the ground truth to create synthetic simulations.

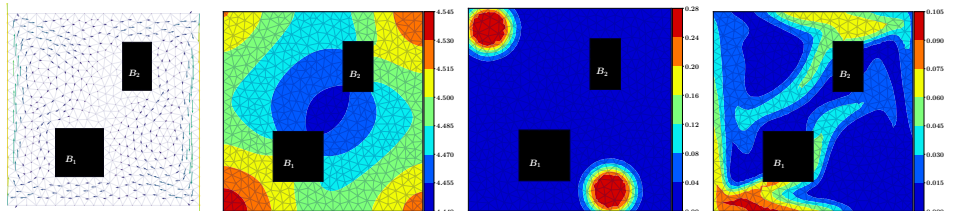


Fig. 2: Advection-diffusion model (4.1). Panels from left to right are (1) the constant velocity field; (2) the prior variance field, that is, the diagonal of the prior covariance matrix; (3) ground truth of the inference parameter; that is, the true initial condition; and (4) the model state at the final simulation time instance $T = 3.6$.

Forward operator, adjoint operator, and the prior. The forward operator \mathbf{F} maps the model parameter θ , here the model initial condition, to the observation space. Specifically, \mathbf{F} represents a forward simulation over the interval $[0, T]$ followed by applying a restriction/observation operator to extract concentrations u at sensor locations at the observation times. The observations are collected along the observation trajectory, and thus the observation operator is time-dependent and is tied to the path as described below. Here \mathbf{F} is linear, and the adjoint is defined as $\mathbf{F}^* = \mathbf{M}^{-1} \mathbf{F}^T$, where \mathbf{M} is the finite-element mass matrix. The prior distribution of the parameter θ is modeled by a Gaussian $\mathcal{N}(\theta_{\text{pr}}, \mathbf{\Gamma}_{\text{pr}})$, where $\mathbf{\Gamma}_{\text{pr}}$ is a discretization of \mathcal{A}^{-2} , with \mathcal{A} being a Laplacian. The prior variance field is plotted in the second panel of Figure 2.

Navigation mesh. We use two navigation meshes (Figure 3): a coarse mesh (left) for exact trajectory analysis and a fine mesh (right). Each node connects to its four nearest neighbors, approximating movement in cardinal directions, with no self-loops. Navigation meshes can be designed to include additional connectivity constraints.

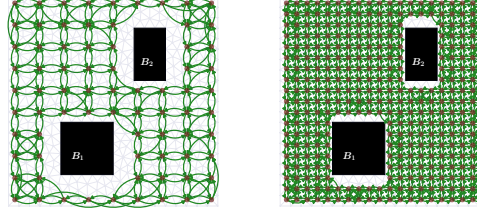


Fig. 3: Navigation meshes used. Left: a coarse mesh with 75 candidate locations (graph vertices/nodes). Right: a fine navigation mesh with 332 nodes.

Trajectory and observational setup. An observation vector \mathbf{y} represents the concentration of the contaminant observed along the trajectory. The observation times are $if\Delta t$, where $\Delta t = 0.2$ is the model simulation timestep; $f > 0$ is the observation temporal frequency; and $i = 1, \dots, n$. Thus, irrespective of f , the trajectory length (number of nodes) is n . For a group of s sensors, the node on the path is the spatial gridpoint at the center of the group, resulting in an observation vector of size $N_{\text{obs}} = s \times n_t$. Here we show results obtained by using only one moving sensor ($s = 1$) yielding scalar observations along the trajectory. In the supplementary material (see Section C) we discuss numerical experiments carried out with $s = 7$ moving sensors.

Observation frequency and path synchronization. Because the design ζ defines spatiotemporal observation locations, the observational path must be synchronized with the model simulation times. The transition from one node to the next occurs at $f\Delta t$. In our setup we use observation frequency $f = 7$ with a trajectory length $n = 7$ nodes when the coarse navigation mesh (Figure 3, left) is used. When the fine navigation mesh (Figure 3, right) is used, the observation frequency is set to $f = 1$, and the trajectory length is $n = 19$ nodes. Thus, both trajectories end up at the same observation time matching the simulation final time of $T = 3.6$. This enables matching the length of traveled paths in both cases to each other.

Bayesian inverse problem. The forward problem $\mathbf{y} = \mathbf{F}(\theta) + \epsilon$ relates the inference parameter θ to the observations \mathbf{y} . The observation error ϵ follows a Gaussian distribution $\mathcal{N}(\mathbf{0}, \mathbf{\Gamma}_{\text{noise}})$, with $\mathbf{\Gamma}_{\text{noise}} \in \mathbb{R}^{N_{\text{obs}} \times N_{\text{obs}}}$ describing spatiotemporal correlations. For simplicity, we assume that observation errors are uncorrelated, with diagonal $\mathbf{\Gamma}_{\text{noise}}$. Observation noise variances are set to 5% of the maximum absolute contaminant concentration at each observation point, estimated from a simulation over $[0, T = 3.6]$ using the true model parameter; see Figure 2.

In this case the posterior is Gaussian $\mathcal{N}(\theta_{\text{post}}^{\mathbf{y}}, \mathbf{\Gamma}_{\text{post}})$ (see, e.g., [6, 36]) with

$$(4.2) \quad \mathbf{\Gamma}_{\text{post}} = (\mathbf{F}^* \mathbf{\Gamma}_{\text{noise}}^{-1} \mathbf{F} + \mathbf{\Gamma}_{\text{pr}}^{-1})^{-1}, \quad \theta_{\text{post}}^{\mathbf{y}} = \mathbf{\Gamma}_{\text{post}} (\mathbf{\Gamma}_{\text{pr}}^{-1} \theta_{\text{pr}} + \mathbf{F}^* \mathbf{\Gamma}_{\text{noise}}^{-1} \mathbf{y}).$$

Initial location and initial policy parameter. The initial policy parameter $\mathbf{p}^{(0)}$ passed to Algorithm 3.3 encodes both the initial point of the trajectory and the admissible navigation directions. A fixed start at node v_i is enforced by setting $p_j =$

δ_{ij} , while multiple admissible starts are handled by assigning nonzero values (e.g., 0.5) to the corresponding entries and zero elsewhere. Here we allow the trajectory to start anywhere on the navigation mesh by setting the initial distribution parameter to $p_i = 0.5, i = 1, \dots, N$. Additional experiments employing a fixed starting point are discussed in the supplementary material in [Section C](#). The transition probabilities p_j^i in all experiments are initialized to 0.5 for all arcs in the navigation mesh. For higher-order policies, the initial lag weights are initialized to $\lambda_i = 1/k, i = 1, \dots, k$, when the weights are allowed to be optimized; otherwise they are modeled by [\(3.19\)](#).

4.2. Utility Function and the OED Optimization Problem. An inverse problem is solved for a given experimental design ζ , and thus ζ is omitted from [\(4.2\)](#). In OED for data acquisition, however, the design affects the observation operator. Hence it modifies the forward operator \mathbf{F} , the adjoint \mathbf{F}^* , and the data noise covariance $\mathbf{\Gamma}_{\text{noise}}$, making the posterior covariance $\mathbf{\Gamma}_{\text{post}} \equiv \mathbf{\Gamma}_{\text{post}}(\zeta)$ a function of the design.

In Bayesian OED an optimal design ζ^{opt} aims to minimize the uncertainty in the solution of the inverse problem, by minimizing a scalar summary of $\mathbf{\Gamma}_{\text{post}}(\zeta)$. Popular optimality criteria include the trace (A-optimal), determinant or log-determinant (D-optimal), and maximum eigenvalue (E-optimal) of the posterior covariance. Here we seek D-optimal paths, with experiments targeting A- and E-optimal paths deferred to [Subsection C.3](#). Thus, the probabilistic OED optimization [Problem 3.2](#) becomes

$$(4.3) \quad \mathbf{p}^{\text{opt}} \in \arg \min_{\zeta \sim \mathbb{P}(\zeta | \mathbf{p})} \mathbb{E}_{\zeta \sim \mathbb{P}(\zeta | \mathbf{p})} [\mathcal{U}(\zeta)]; \quad \mathcal{U}(\zeta) = \log \det (\mathbf{\Gamma}_{\text{post}}(\zeta)).$$

Unless stated otherwise, we use the stochastic gradient with optimal baseline estimate [\(3.23\)](#) with batch size $N_b = 1$. Justification of this choice is discussed in [Subsection 4.4](#). All experiments use a maximum of 300 iterations, and [Algorithm 3.3](#) terminates early if the parameter update norm $\|\mathbf{p}^{(i+1)} - \mathbf{p}^{(i)}\|_2$ falls below 10^{-12} .

4.3. Results with Coarse Navigation Mesh and 1 Moving Sensor. This experiment employs the coarse navigation mesh in [Figure 3](#) (left). The trajectory length is set to $n = 7$ nodes (observation time points), and the observation frequency is set to $3\Delta t$, with $\Delta t = 0.2$ being the model simulation step. This is a simplified setup that allows us to enumerate all *feasible* paths and thus enables sketching the distribution of the utility function \mathcal{U} , evaluating the exact objective $\mathbb{E}[\mathcal{U}]$ and the exact gradient $\nabla_{\mathbf{p}} \mathbb{E}[\mathcal{U}]$, and finding the global optima for benchmarking.

4.3.1. Benchmark: Utility Function Distribution and Global Optimum. The support cardinality—total number of feasible paths—in this case is 307, 200, with objective values \mathcal{U} displayed in [Figure 4](#) (left). The utility evaluation for each trajectory took (on average) 0.3 seconds, totaling approximately 27 hours to generate brute-force results on a non-parallel platform. The global optimum path is unique (shown in [Figure 4](#), right) with minimum value -21714.37 . The corresponding posterior variance field (diagonal of $\mathbf{\Gamma}_{\text{post}}$ in [\(4.2\)](#)) exhibits a substantial reduction in uncertainty relative to the prior variance field in [Figure 2](#).

Although the global optimum is unique, many trajectories attain near-optimal utility \mathcal{U} , motivating exploration of the lower tail (e.g., lowest 1% values), as in [Figure 4](#). Accordingly, our goal is to learn a probabilistic policy that samples trajectories with objective/utility values close to the global optimum.

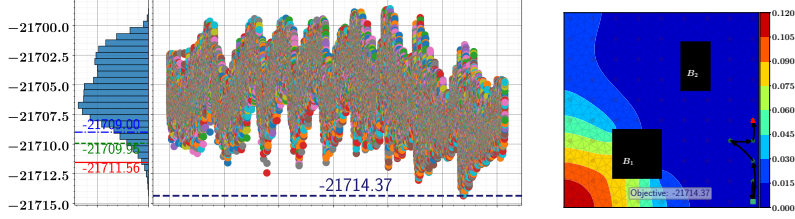


Fig. 4: Brute-force results for the coarse experiment. Left: The values and the distribution of the utility function \mathcal{U} (4.3) for feasible paths. Each path is assigned a unique index (on the x-axis) with a colored circle on the y-axis representing the corresponding utility value. The utility function distribution is binned horizontally with the first, second, and third quantiles are displayed. Right: The global optimum (with optimal value -21714.37) along with the corresponding posterior variance field.

4.3.2. Results with the First-Order Policy. We start by discussing the results of Algorithm 3.3 with the first-order policy (Definition 3.1).

Figure 5 (left) shows the utility function \mathcal{U} value evaluated at the samples generated at each iteration of the optimization procedure. The algorithm identifies the rightmost side of the domain—particularly near building B_2 and the lower-right corner—as having higher chances of optimizing the objective when a path is initiated in these locations; see Figure 5 (middle). The optimal initial parameters (middle) are sparse, and the optimal transition parameters (right) are likewise sparse across nodes, highlighting preferred navigation directions. Figure 5 (left) shows that the policy updates rapidly reduce the average objective, with most improvement in early iterations, suggesting early stopping is possible. In contrast, uniform random sampling fails to capture the lower tail of the utility distribution, even in this simplified setup.

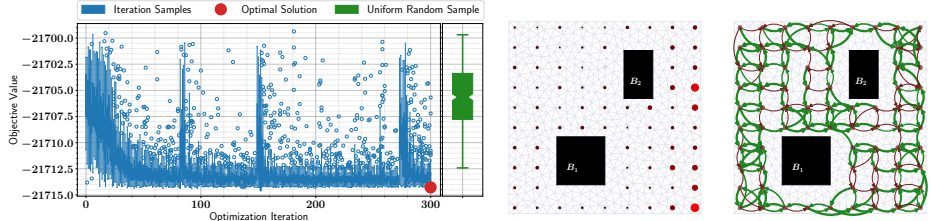


Fig. 5: Results of Algorithm 3.3 with the first-order policy (Definition 3.1). Left: utility function \mathcal{U} (4.3) evaluated at the samples generated at each iteration, with the optimal value shown as a red circle. A boxplot of \mathcal{U} values corresponding to 500 uniformly sampled—with parameters equal 0.5; paths are also displayed. Middle: the optimal initial parameters π_i plotted as circles centered at the corresponding mesh nodes, with the circle size proportional to the magnitude of the parameter. Right: the optimal transition parameters p_j^i with line widths proportional to the magnitude of p_j^i values. Maroon indicates values below 0.5, and green indicates otherwise.

The solution (Figure 6, left) returned by Algorithm 3.3 is associated with an objective value that is close (but not identical) to the global optimal value as shown in Figure 6 (left). Moreover, the samples generated from the optimal policy explore the space near the global optimal value, as indicated by the samples shown in Figure 6. Additionally, the posterior velocity field given the optimal trajectory and the other

optimal policy samples are almost identical to the posterior velocity field associated with the global optimal solution shown in Figure 4 (right). This aligns well with our objective to generate a policy that explores the lower tail of the utility distribution. Although global optimality is not guaranteed, with more samples from the optimal policy we were able to recover the global optimum; the results are omitted for brevity.

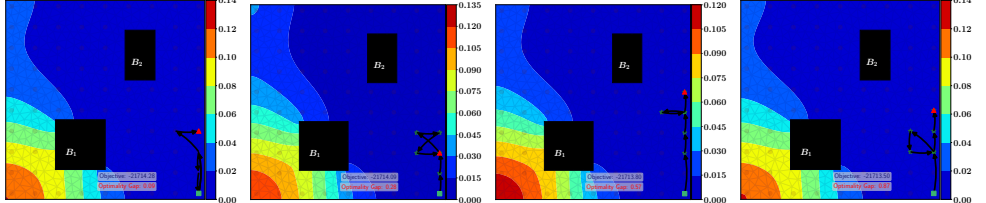


Fig. 6: Optimal trajectory followed by 3 samples from the optimal policy in Figure 5.

4.3.3. Results with the Higher-Order Policies. We present results of Algorithm 3.3 with higher-order policies (Definition 3.2, Definition 3.3), comparing optimized versus fixed lag weights (via (3.19)) for orders $k = 3$ and $k = 5$, respectively.

Results obtained by using Definition 3.2 with orders $k = 3, k = 5$, are shown in Figure 7 and Figure 8, respectively. The results indicate that optimizing lag weights slightly increases optimizer instability. While it explores the second percentile of the utility distribution (see Figure 4, left), this higher-order model generally underperforms the first-order model except for higher-order $k = 5$ and fixed lag weights.

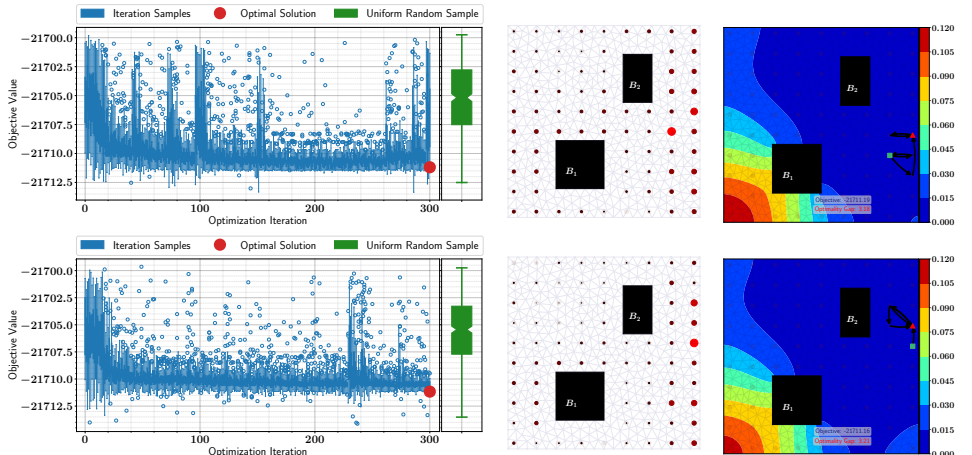


Fig. 7: Results of Algorithm 3.3 with the higher-order policy model Definition 3.2 with order $k = 3$. The first row shows results with lag weights being optimized, and the second row shows results with lag weights modeled by (3.19).

Results obtained by using Definition 3.3 with order $k = 3$ and $k = 5$ are shown in Figure 9 and Figure 10, respectively. These results suggest that the two higher-order policy models proposed behave similarly in this setup and yield optimal paths associated with posterior variance fields similar to that of the global optimum.

4.4. On the Necessity of a Baseline. The baseline is critical for reducing the variability of the stochastic estimator and enhancing optimization efficiency. We em-

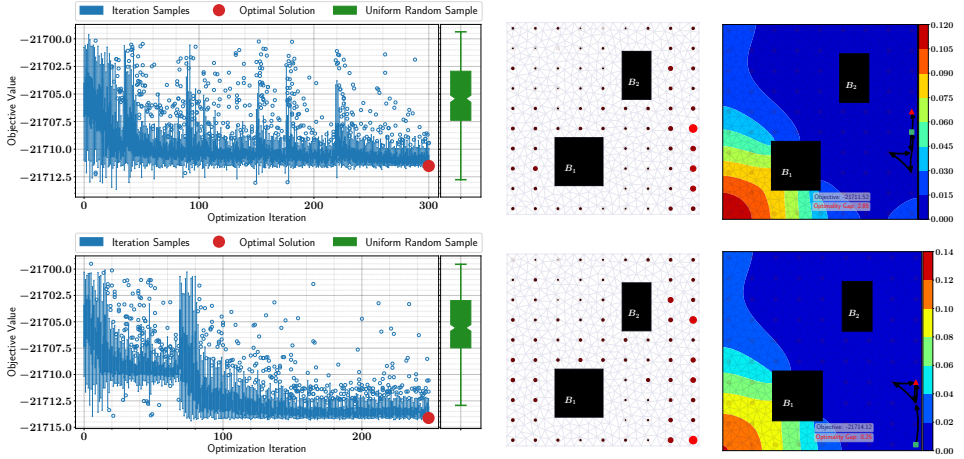


Fig. 8: Similar to Figure 7. Here the policy order is set to $k = 5$.

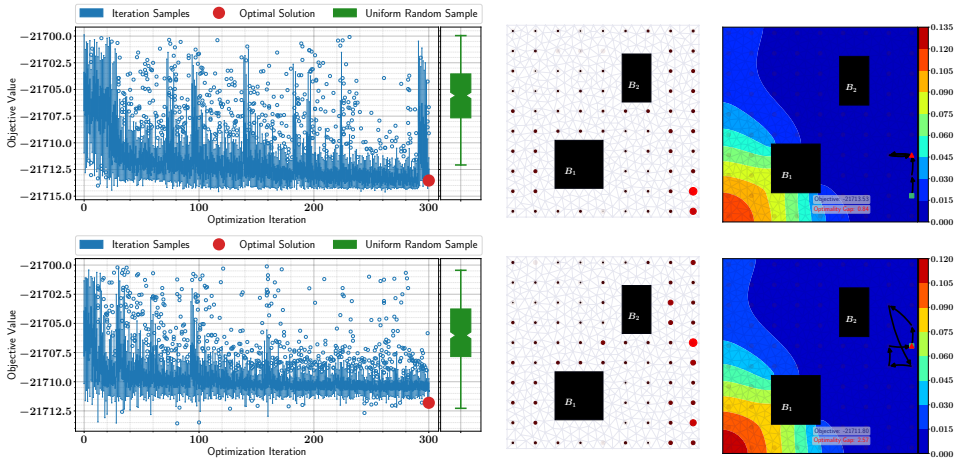


Fig. 9: Similar to Figure 7. Here the higher-order policy (Definition 3.3) is used.

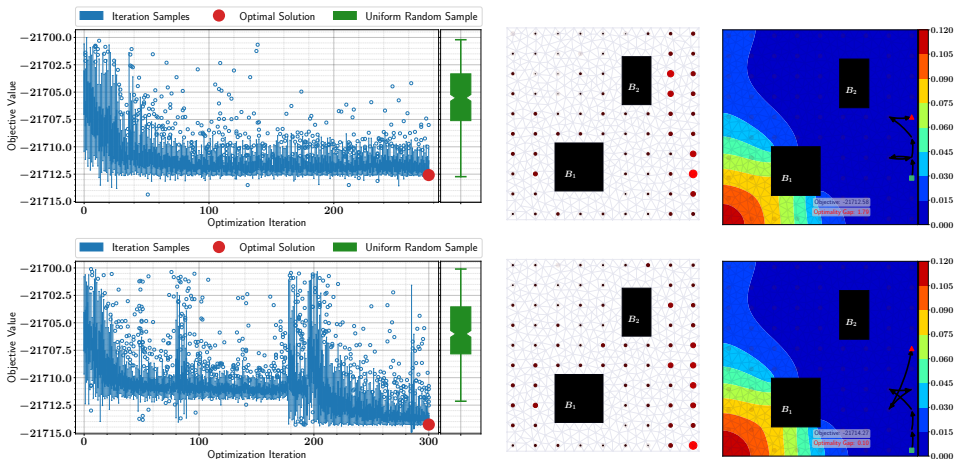


Fig. 10: Similar to Figure 9. Here the policy order is set to $k = 5$.

pirically assess stochastic gradient quality, with and without a baseline. We employ the same setup in [Subsection 4.3.2](#), and we use the brute-force results in [Subsection 4.3.1](#) to compute the exact gradient \mathbf{g} (2.3a) and the error of the stochastic gradient. For fixed sample sizes, stochastic gradients $\hat{\mathbf{g}}$ with and without a baseline are replicated 32 times to estimate the errors relative to the exact gradient \mathbf{g} , across varying ensemble N_{ens} and baseline batch N_b sizes. The errors and variances of the stochastic gradient estimator are summarized in [Figure 11](#) and [Figure 12](#), respectively.

[Figure 11](#) shows that the mean error is centered around 0 reflecting the unbiasedness of the stochastic gradient with or without a baseline. Increasing the sample size N_{ens} , by definition, reduces variability but at a high computational cost. In contrast, using a baseline greatly reduces variance even with a batch size of $N_b = 1$, as shown in [Figure 12](#), and incurs no additional cost.

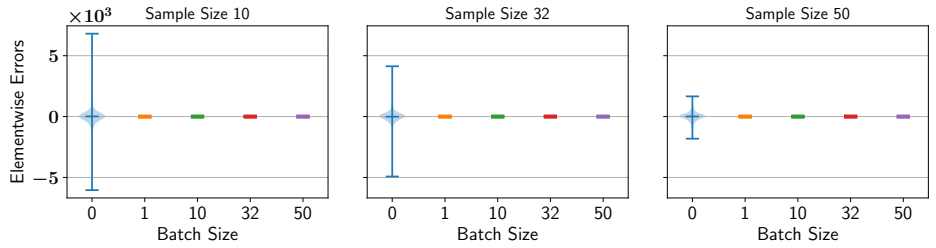


Fig. 11: Stochastic gradient elementwise errors $\hat{\mathbf{g}} - \mathbf{g}$ averaged across 32 replicas for sample sizes N_{ens} set to 10 (left), 32 (middle), and 50 (right), respectively. A uniformly sampled parameter instance $\mathbf{p} \in [0, 1]^{N_p}$ is used. For each sample size, the stochastic gradient is computed without baseline $b = 0$ (batch size 0) and with optimal baseline estimate (3.23d) by using batch sizes $N_b = 1, 10, 32, 50$, respectively.

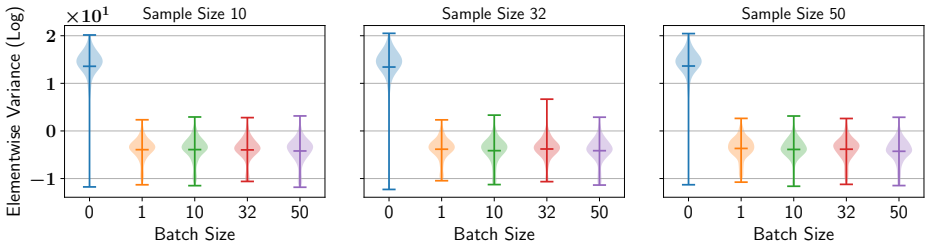


Fig. 12: Similar to [Figure 11](#). Here elementwise variances (log scale) are plotted.

To further illustrate the baseline's impact, [Figure 13](#) shows results for the benchmark experiment in [Subsection 4.3.1](#) without using a baseline. With the small sample size $N_{\text{ens}} = 32$, high gradient variance degrades policy updates, preventing consistent reduction of the expected objective. Although a near-optimal path (right) is retrieved as evident by the posterior variance, this is incidental, as the initial distribution is poorly optimized (middle) and the resulting policy remains highly variable (left).

The results in [Figure 12](#) and [Figure 13](#) clearly show that employing the baseline is critical for the performance of the optimization procedure.

4.5. Results with Fine Navigation Mesh and 1 Moving Sensor. This experiment uses the fine navigation mesh ([Figure 3](#), right), with trajectories of $n = 19$ nodes and observation frequency $f = 1$, yielding 19 scalar observations along the path.

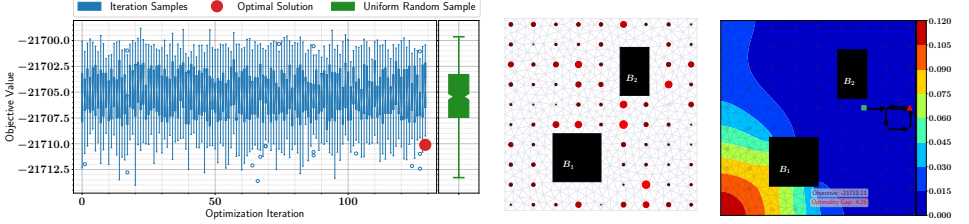


Fig. 13: Results of the experiment in Subsection 4.3.2 without employing a baseline.

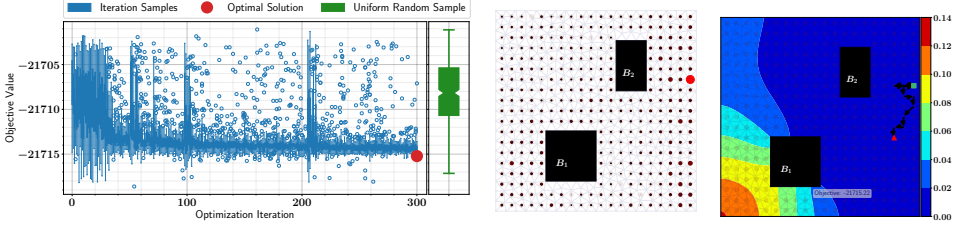


Fig. 14: Results of Algorithm 3.3 with the first-order policy (Definition 3.1) applied to the fine navigation mesh (Figure 3, right) with trajectory length of $n = 19$.

Results obtained by using the first-order policy (Definition 3.1) are shown in Figure 14. Results obtained by using the higher-order policy (Definition 3.2) are shown in Figure 15 and Figure 16. Results obtained by using the generalized higher-order policy (Definition 3.3) are shown in Figure 17 and Figure 18.

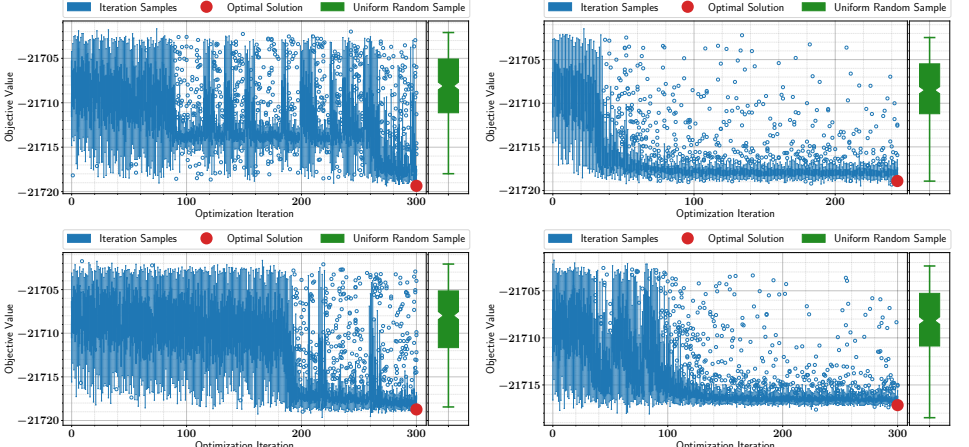


Fig. 15: Results of Algorithm 3.3 with the higher-order policy (Definition 3.2) applied to the fine navigation mesh (Figure 3, right) with trajectory length of $n = 19$. Results are shown for policy order $k = 3$ (first row) and $k = 5$ (second row). The first column shows results with lag weights being calibrated by the optimization procedure, and the second row column shows results with lag weights modeled by (3.19).

The results shown here suggest that the higher-order policies both enable achieving lower objective values than the first-order policy, with optimal solutions closer to the global optimum of the experiment with coarse mesh; see Figure 4 (right). Similar to the case of the coarse mesh in Subsection 4.3, for a higher order the optimization

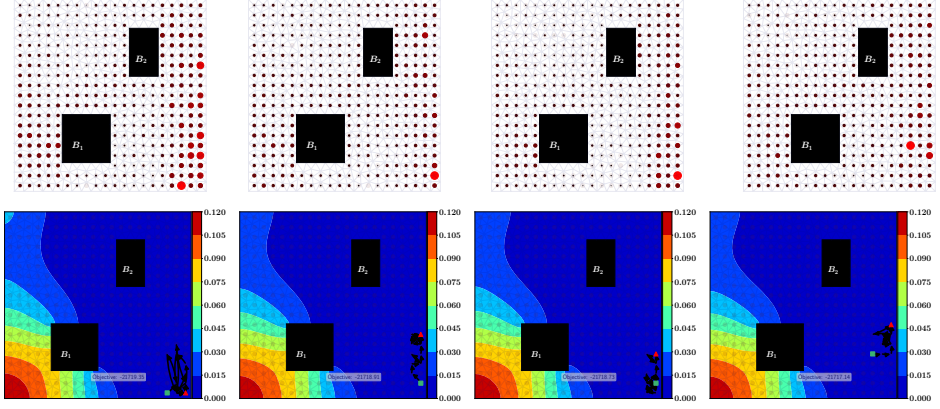


Fig. 16: Optimal initial distribution parameters (top row) and optimal trajectories (bottom row) corresponding to Figure 15. In each row, the first two panels match the first row of that figure, followed by panels corresponding to its second row.

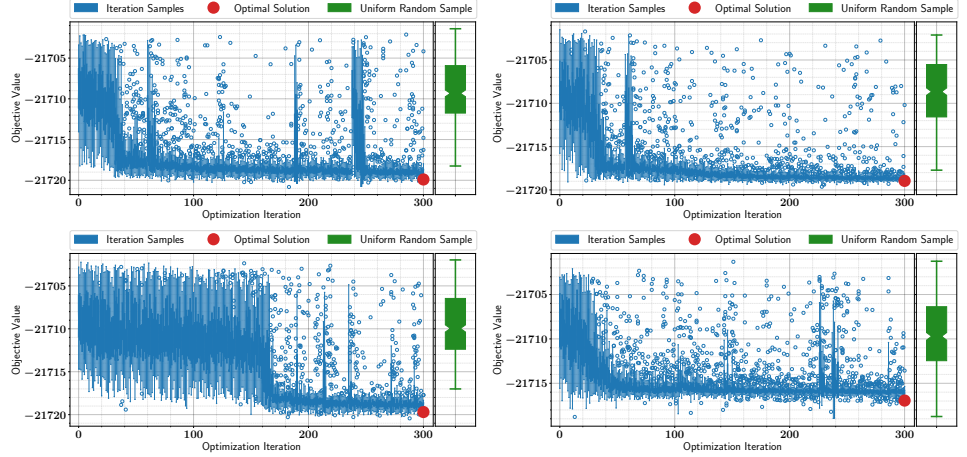


Fig. 17: Similar to Figure 15. Here the policy given by Definition 3.3 is used.

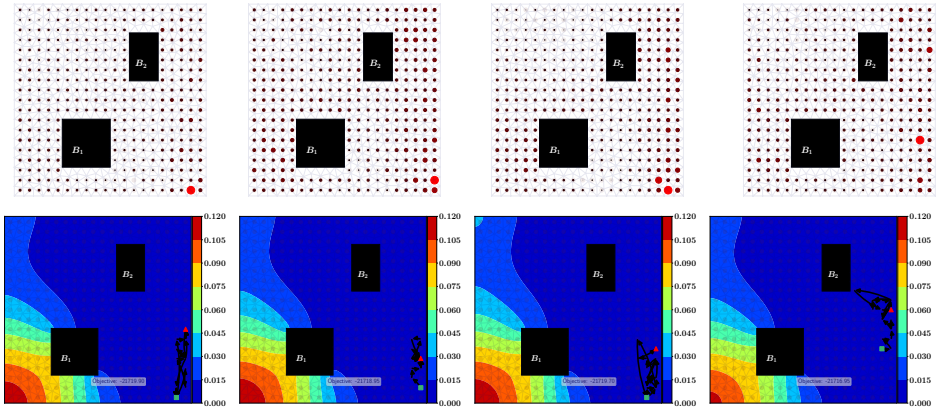


Fig. 18: Optimal initial parameters and trajectories corresponding to Figure 17.

procedure takes more time to reduce the average objective. Additionally, the modeled lag weights (3.19) stabilize the optimizer more than when the lag weights are calibrated. All higher-order configurations here identify the bottom right corner of the domain as the favorable initial region of the path and return an optimal design with similar objective values. The generalized higher-order model with lag-dependent transitions (Definition 3.3), however, yields slightly better performance than does the case of the higher-order policy (Definition 3.2). This, however, comes at a higher computational cost, as discussed in Subsection 3.2.2.

We conclude by noting that different OED utility functions can yield optimal trajectories with distinct shapes, as supported by the results here and in Section C. Nevertheless, across all choices of \mathcal{U} , the optimal trajectories lie in regions of minimal activity, reflecting reduced uncertainty induced by the construction of the synthetic data and noise covariance here. Utility functions may also be designed to target specific objectives, such as prediction accuracy for tracking concentration modes, and their choice is independent of the proposed path optimization framework.

5. Discussion and Concluding Remarks. This work presents an efficient probabilistic approach for path optimal experimental design, such as optimizing moving sensors path. The path OED problem is formulated as discrete optimization on a navigation mesh, treating the utility function as a black box, and is reformulated as a probabilistic optimization over policy parameters. The approach is broadly applicable to path OED problems on navigation meshes and accommodates any utility function.

In this work we propose three parametric policies to model the probability distribution of the design/path based on first- and higher-order Markov chains. The experiments discussed in Section 4 along with the additional results in the supplementary material in Section C indicate that the first-order policy (Definition 3.1) yields acceptable results and generally converges to a policy that explores the lower tail of the OED utility function distribution. The generalized higher-order policy with lag-dependent transitions (Definition 3.3) achieves better results than does the higher-order policy with lag-independent transitions (Definition 3.2) at a slightly higher computational cost. The higher-order policies are generally more flexible; but without freezing the lag weights, the optimizer can be unstable and may require more iterations to converge. Moreover, they can allow the generation of trajectories involving successive nodes violating connectivity in the navigation mesh. To mitigate such an effect, one can increase the fineness of the mesh, use a small order (e.g., $k = 3$), or use a fast-decaying series of lag weights to enforce much lower weight on the past.

The empirical study shows that the optimization procedure behaves similarly for various choices of the OED utility function: overall the optimizer quickly reduces the average value of the utility function, converging to the tail of the utility function distribution. This enables exploring the space near global optima. Reaching the global optimal value, however, is not guaranteed.

While we provide insight on the choice between the proposed policies, and the policy order, these remain as user choices. Alternatively, one can identify the best model and order, for example, based on some model choice or information criterion. This, however, is outside the scope of this work and will be explored in the future. The proposed policies do not explicitly enforce path smoothness, but this can be indirectly encouraged through penalizing the utility function or by fitting smooth curves between nodes on a coarse mesh. Enforcing history-dependent constraints,

such as no-visit constraints, is left for future work.

Appendix A. Proofs of Propositions in Subsection 3.1.

Proof of Proposition 3.1. The log-policy gradient (3.10a) requires defining the gradients of the initial distribution $\mathbb{P}(\zeta_1)$ (first term) and the transition distribution $\mathbb{P}(\zeta_{t+1} | \zeta_t)$ (second term). The parameter vector contains initial parameters p_i and transition parameters p_j^i . Moreover, the initial distribution does not depend on the transition parameters, and the transition distribution does not depend on the initial parameters. Thus, it suffices to develop the partial derivatives $\frac{\partial \log \pi_i}{\partial p_j}$ and $\frac{\partial \log \pi_j^i}{\partial p_m^i}$:

$$(A.1a) \quad \frac{\partial \log \pi_i}{\partial p_j} \equiv \frac{\partial \log \mathbb{P}(\zeta_1 = v_i)}{\partial p_j} \stackrel{(3.5)}{=} \frac{\partial}{\partial p_j} \left(\log w_i - \log \left(\sum_{k=1}^N w_k \right) \right)$$

$$(A.1b) \quad = \frac{1}{w_i} \frac{\partial w_i}{\partial p_j} - \frac{\sum_{k=1}^N \frac{\partial w_k}{\partial p_j}}{\sum_{k=1}^N w_k} = \frac{1}{w_i} \frac{\partial w_i}{\partial p_j} - \frac{\frac{\partial w_j}{\partial p_j}}{\sum_{k=1}^N w_k} \stackrel{(3.5)}{=} \frac{\delta_{ij} \partial w_j}{w_j \partial p_j} - \frac{\partial w_j}{\sum_{k=1}^N w_k}$$

$$(A.1c) \quad = \frac{\partial w_j}{\partial p_j} \left(\frac{\delta_{ij}}{w_j} - \frac{1}{\sum_{k=1}^N w_k} \right) = \frac{1}{(1-p_j)^2} \left(\frac{\delta_{ij}}{w_j} - \frac{1}{\sum_{k=1}^N w_k} \right),$$

where δ_{in} is the Kronecker delta function. Similarly we derive (3.10c):

$$(A.2) \quad \frac{\partial \log \pi_j^i}{\partial p_m^l} = \frac{\delta_{jm} \partial w_m^l}{w_m^l \partial p_m^l} - \frac{\frac{\partial w_m^l}{\partial p_m^l}}{\sum_{k=1}^N w_k^l} = \frac{\delta_{il}}{(1-p_m^l)^2} \left(\frac{\delta_{jm}}{w_m^l} - \frac{1}{\sum_{k=1}^N w_k^l} \right). \quad \square$$

Proof of Proposition 3.2. The policy parameter (3.14b) consists of the initial parameters, the transition parameters, and the lag parameters. Thus, the gradient of the log-policy is given by the general form (3.15a). From (3.14a), it follows that

$$(A.3) \quad \log \mathbb{P}(\zeta) = \log \mathbb{P}(\zeta_1) + \sum_{t=1}^{k-1} \log \mathbb{P}(\zeta_{t+1} | \zeta_t) + \sum_{t=k}^{n-1} \log \left(\sum_{i=1}^k \lambda_i \mathbb{P}(\zeta_{t+1} | \zeta_{t+1-i}) \right).$$

Only the first term in (A.3) depends on the initial parameters, thus $\frac{\partial \log \mathbb{P}(\zeta)}{\partial p_j} = \frac{\partial \log \mathbb{P}(\zeta_1)}{\partial p_j}$ which proves (3.15b). Conversely, only the second and third terms in (A.3) depend on the transition parameters, which proves (3.15c). The derivative with respect to the lag parameters (3.15d) is obtained from the third term in (A.3) as follows

$$(A.4) \quad \begin{aligned} \frac{\partial \log \mathbb{P}(\zeta)}{\partial \lambda_l} &= \frac{\partial}{\partial \lambda_l} \sum_{t=k}^{n-1} \log \left(\sum_{i=1}^k \lambda_i \mathbb{P}(\zeta_{t+1} | \zeta_{t+1-i}) \right) \\ &= \sum_{t=k}^{n-1} \frac{\sum_{i=1}^k \lambda_i \frac{\partial \mathbb{P}(\zeta_{t+1} | \zeta_{t+1-i})}{\partial \lambda_l}}{\sum_{i=1}^k \lambda_i \mathbb{P}(\zeta_{t+1} | \zeta_{t+1-i})} = \sum_{t=k}^{n-1} \frac{\mathbb{P}(\zeta_{t+1} | \zeta_{t+1-l})}{\sum_{i=1}^k \lambda_i \mathbb{P}(\zeta_{t+1} | \zeta_{t+1-i})}. \end{aligned} \quad \square$$

Proof of Proposition 3.3. The proof is similar to that of Proposition 3.3 with higher-order transitions used. Specifically, from (3.17a) it follows that

$$(A.5) \quad \log \mathbb{P}(\zeta) = \log \mathbb{P}(\zeta_1) + \sum_{t=1}^{k-1} \log \mathbb{P}(\zeta_{t+1} | \zeta_t) + \sum_{t=k}^{n-1} \log \left(\sum_{i=1}^k \lambda_i \mathbb{P}^{(i)}(\zeta_{t+1} | \zeta_{t+1-i}) \right).$$

Because the first terms in (A.3) and (A.5) are identical, the derivative of the log-policy with respect to the initial parameters holds here as well, which proves (3.18b). Conversely, the third term in (A.5) replaces the first-order transitions $\mathbb{P}(\zeta_{t+1} | \zeta_{t+1-i})$ with the higher-order transitions $\mathbb{P}^{(i)}(\zeta_{t+1} | \zeta_{t+1-i})$. This modifies the derivative of the log-policy with respect to the transition and the lag parameters as follows. The derivative with respect to transition parameters (3.18c) is

$$(A.6) \quad \begin{aligned} \frac{\partial \log \mathbb{P}(\zeta)}{\partial p_m^l} &= \sum_{t=1}^{k-1} \frac{\partial \log \mathbb{P}(\zeta_{t+1} | \zeta_t)}{\partial p_m^l} + \frac{\partial}{\partial p_m^l} \sum_{t=k}^{n-1} \log \left(\sum_{i=1}^k \lambda_i \mathbb{P}^{(i)}(\zeta_{t+1} | \zeta_{t+1-i}) \right) \\ &= \sum_{t=1}^{k-1} \frac{\partial \log \mathbb{P}(\zeta_{t+1} | \zeta_t)}{\partial p_m^l} + \sum_{t=k}^{n-1} \frac{\sum_{i=1}^k \lambda_i \frac{\partial}{\partial p_m^l} \mathbb{P}^{(i)}(\zeta_{t+1} | \zeta_{t+1-i})}{\sum_{i=1}^k \lambda_i \mathbb{P}^{(i)}(\zeta_{t+1} | \zeta_{t+1-i})}. \end{aligned}$$

The derivative with respect to the lag parameters (3.18d) is obtained directly by differentiating the third term in (A.5) since the first two terms are independent of these parameters. Finally (3.18e) follows by differentiating the higher-order transition probabilities (3.17e) with respect to the first-order transition parameters. \square

This supplementary material provides a detailed explanation of the computations under the probabilistic policies proposed in Subsection 3.1, and provides additional numerical experiments to complement the empirical analysis discussed in Section 4.

Appendix B. Illustrative Example. Here we provide an example with detailed computations under the parametric probabilistic policies proposed by Definition 3.1, Definition 3.2, and Definition 3.3, respectively.

Consider the simplified navigation mesh (transition graph) shown in Figure 19, with the first-order transition parameters p_j^i indicated on the corresponding arcs.

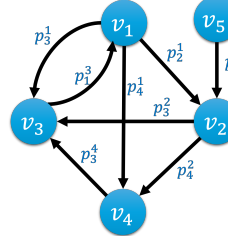


Fig. 19: Directed graph describing a simple navigation mesh. The graph consists of $N = 5$ nodes v_1, \dots, v_5 with transition parameters p_j^i describing the probability of moving from node v_i to node v_j displayed on the respective arcs (v_i, v_j) .

The proposed probabilistic policies require the initial parameters p_i that define the probability of a path starting from node v_i and the transition parameters p_j^i that

encode the probability of moving from node v_i to node v_j . In this example these parameters are given by

$$(B.1a) \quad [p_i]_{i=1,\dots,5} := (p_1, p_2, p_3, p_4, p_5) ,$$

$$(B.1b) \quad [p_j^i]_{i,j=1,\dots,5} := \begin{matrix} & \begin{matrix} v_1 & v_2 & v_3 & v_4 & v_5 \end{matrix} \\ \begin{matrix} v_1 \\ v_2 \\ v_3 \\ v_4 \\ v_5 \end{matrix} & \begin{bmatrix} 0 & p_2^1 & p_3^1 & p_4^1 & 0 \\ 0 & 0 & p_3^2 & p_4^2 & 0 \\ p_1^3 & 0 & 0 & 0 & 0 \\ 0 & 0 & p_1^4 & 0 & 0 \\ 0 & p_2^5 & 0 & 0 & 0 \end{bmatrix} \end{matrix} ,$$

where the transition parameters (as well as connectivity) are induced from the navigation mesh in [Figure 19](#). According to (3.9b), for example, the parameter vector \mathbf{p} of the first-order policy takes the form

$$(B.2) \quad \mathbf{p} = \left(\underbrace{p_1, p_2, p_3, p_4, p_5}_{\text{initial parameters}}; \underbrace{p_2^1, p_3^1, p_4^1; p_3^2, p_4^2; p_1^3; p_1^4; p_2^5}_{\text{transition parameters}} \right) ,$$

where all zero-valued transition parameters are removed from the parameter vector because they never change.

When implemented, however, this efficient representation (B.2) requires keeping a connectivity matrix and an indexing scheme to enable efficient development of the gradient of the log-policy with respect to the parameter vector. This approach is followed in the implementations available through the PyOED framework [18]. Specifically, the code—publicly available through the PyOED package repository [5]—with implementations of the proposed policies is available under the subpackage `pyoed.stats.distributions`. For clarity, however, here we keep the parameters in their original forms (B.1).

The policy parameters (B.1) are used to define initial w_i and transition w_j^i weights, respectively:

$$(B.3a) \quad w_i = \frac{p_i}{1 - p_i} , \quad i = 1, \dots, 5 ,$$

$$(B.3b) \quad w_j^i = \frac{p_j^i}{1 - p_j^i} , \quad i = 1, \dots, 5 , \quad j = 1, \dots, 5 .$$

From (B.1) and (B.3), the initial and transition weights are given by

$$(B.4a) \quad [w_i]_{i=1,\dots,5} = \left(\frac{p_1}{1 - p_1}, \frac{p_2}{1 - p_2}, \frac{p_3}{1 - p_3}, \frac{p_4}{1 - p_4}, \frac{p_5}{1 - p_5} \right) ,$$

$$(B.4b) \quad [w_j^i]_{i,j=1,\dots,5} = \begin{matrix} & \begin{matrix} v_1 & v_2 & v_3 & v_4 & v_5 \end{matrix} \\ \begin{matrix} v_1 \\ v_2 \\ v_3 \\ v_4 \\ v_5 \end{matrix} & \begin{bmatrix} 0 & \frac{p_2^1}{1-p_2^1} & \frac{p_3^1}{1-p_3^1} & \frac{p_4^1}{1-p_4^1} & 0 \\ 0 & 0 & \frac{p_3^2}{1-p_3^2} & \frac{p_4^2}{1-p_4^2} & 0 \\ \frac{p_1^3}{1-p_1^3} & 0 & 0 & 0 & 0 \\ 0 & 0 & \frac{p_3^4}{1-p_3^4} & 0 & 0 \\ 0 & \frac{p_2^5}{1-p_2^5} & 0 & 0 & 0 \end{bmatrix} \end{matrix} ,$$

Common to the three policies proposed in this work are the initial (inclusion) probabilities $\pi^i \equiv \mathbb{P}(\zeta_1 = v_i)$ (3.5) and the first-order transition probabilities $\pi_j^i \equiv \mathbb{P}(\zeta_{t+1} = v_j | \zeta_t = v_i)$ (3.8) for any positive integer (time) $t > 0$. From (B.4) it follows that

$$(B.5a) \quad [\pi_i]_{i=1,\dots,5} = \frac{1}{\sum_{i=1}^5 \frac{p_i}{1-p_i}} \left(\frac{p_1}{1-p_1}, \dots, \frac{p_5}{1-p_5} \right)$$

$$(B.5b) \quad [\pi_j^i]_{i,j=1,\dots,5} = \begin{matrix} & v_1 & v_2 & v_3 & v_4 & v_5 \\ \begin{matrix} v_1 \\ v_2 \\ v_3 \\ v_4 \\ v_5 \end{matrix} & \begin{bmatrix} 0 & \frac{w_2^1}{w_2^1 + w_3^1 + w_4^1} & \frac{w_3^1}{w_2^1 + w_3^1 + w_4^1} & \frac{w_4^1}{w_2^1 + w_3^1 + w_4^1} & 0 \\ 0 & 0 & \frac{w_3^2}{w_3^2 + w_4^2} & \frac{w_4^2}{w_3^2 + w_4^2} & 0 \\ 1 & 0 & 0 & 0 & 0 \\ 0 & 0 & 1 & 0 & 0 \\ 0 & 1 & 0 & 0 & 0 \end{bmatrix} \end{matrix}.$$

Trajectory and Distribution Parameter. Without loss of generality and for simplicity we consider the case of a trajectory of length $n = 3$ nodes. For the higher-order policy models, we set the policy order to $k = 2$. Since the path consists of only $n = 3$ nodes, the memory here involves the full path. We also assume the lag parameters are modeled by $\lambda_1 = \frac{2}{3}, \lambda_2 = \frac{1}{3}$ as defined by (3.19).

As a numerical example, we assign the following values to the initial and the first-order transition parameters:

$$(B.6a) \quad [p_i]_{i=1,\dots,5} = (1/2, 1/2, 1/2, 1/2, 1/2),$$

$$(B.6b) \quad [p_j^i]_{i,j=1,\dots,5} = \begin{matrix} & v_1 & v_2 & v_3 & v_4 & v_5 \\ \begin{matrix} v_1 \\ v_2 \\ v_3 \\ v_4 \\ v_5 \end{matrix} & \begin{bmatrix} 0 & 1/2 & 1/2 & 4/5 & 0 \\ 0 & 0 & 1/2 & 1/2 & 0 \\ 1/2 & 0 & 0 & 0 & 0 \\ 0 & 0 & 1/2 & 0 & 0 \\ 0 & 1/2 & 0 & 0 & 0 \end{bmatrix} \end{matrix},$$

resulting in the following initial and transition weights:

$$(B.7a) \quad [w_i]_{i=1,\dots,5} \stackrel{(B.4a)}{=} (1, 1, 1, 1, 1),$$

$$(B.7b) \quad [w_j^i]_{i,j=1,\dots,5} \stackrel{(B.4b)}{=} \begin{matrix} & v_1 & v_2 & v_3 & v_4 & v_5 \\ \begin{matrix} v_1 \\ v_2 \\ v_3 \\ v_4 \\ v_5 \end{matrix} & \begin{bmatrix} 0 & 1 & 1 & 4 & 0 \\ 0 & 0 & 1 & 1 & 0 \\ 1 & 0 & 0 & 0 & 0 \\ 0 & 0 & 1 & 0 & 0 \\ 0 & 1 & 0 & 0 & 0 \end{bmatrix} \end{matrix}.$$

The initial and transition probabilities are thus given by

$$(B.8a) \quad [\pi_i]_{i=1,\dots,5} \stackrel{(B.5a)}{=} \left(\frac{1}{5}, \frac{1}{5}, \frac{1}{5}, \frac{1}{5}, \frac{1}{5} \right),$$

$$(B.8b) \quad [\pi_j^i]_{i,j=1,\dots,5} \stackrel{(B.5b)}{=} \begin{bmatrix} v_1 & v_2 & v_3 & v_4 & v_5 \\ v_1 & 0 & 1/6 & 1/6 & 4/6 & 0 \\ v_2 & 0 & 0 & 1/2 & 1/2 & 0 \\ v_3 & 1 & 0 & 0 & 0 & 0 \\ v_4 & 0 & 0 & 1 & 0 & 0 \\ v_5 & 0 & 1 & 0 & 0 & 0 \end{bmatrix}.$$

As expected, the initial probabilities add up to 1, and each row of the transition probability matrix also sums up to 1. Therefore, for any set of Bernoulli parameters satisfying the box constraints $\pi_i \in [0, 1]$, $\pi_j^i \in [0, 1]$, $\forall i, j = 1, \dots, N$, we can evaluate the initial or the transition distribution/probabilities with automatic satisfaction of the probability distribution constraints.

In what follows we evaluate the probability distribution for each of the policy models proposed in this work.

B.1. First-Order Policy. We first discuss the generation of the support and then evaluate the probabilities for each path in the support.

Distribution support. Since the initial parameter (B.6a) does not include any zeros, the trajectory can start at any of the 5 nodes on the navigation mesh (Figure 19). We begin by listing all trajectories starting with $\zeta_1 = v_1$. Since this is a first-order model, we use the first-order transitions to define the next candidate nodes on the graph. Specifically, starting at v_1 , the next node—by inspecting the transition matrix or the navigation mesh—can be v_2 , v_3 , or v_4 . All these are allowed because the conditional transition parameters p_2^1, p_3^1, p_4^1 are all nonzero. Nonzero parameters guarantee nonzero probabilities, and thus $\pi_2^1, \pi_3^1, \pi_4^1$ are all positive.

Thus, all trajectories of length $n = 2$ starting with $\zeta_1 = v_1$ are

$$(B.9) \quad (\zeta_1 = v_1, \zeta_2) \in \{(v_1, v_2), (v_1, v_3), (v_1, v_4)\},$$

which are then expanded recursively to generate all paths of length 3 starting with $\zeta_1 = v_1$.

From v_2 a sensor is allowed to move to v_3, v_4 . Thus the trajectory (v_1, v_2) can be expanded to two feasible trajectories $\{(v_1, v_2, v_3), (v_1, v_2, v_4)\}$. Similarly, moving from v_3 is allowed to v_1 , and v_4 is allowed to transition only to v_3 . Adding these possible choices expands the trajectories of length 2 starting with $\zeta_1 = v_1$ to the following trajectories of length 3 starting with the same node $\zeta_1 = v_1$:

$$(B.10) \quad (\zeta_1 = v_1, \zeta_2, \zeta_3) \in \{(v_1, v_2, v_3), (v_1, v_2, v_4), (v_1, v_3, v_1), (v_1, v_4, v_3)\}.$$

By following the same strategy for the other starting points $\zeta_1 \in \{v_2, v_3, v_4, v_5\}$, respectively, the distribution support consisting of 12 feasible paths $(\zeta_1, \zeta_2, \zeta_3)$ of length $n = 3$ can be generated.

Probability mass function. From [Definition 3.1](#), the probability distribution (mass function) evaluated at all feasible trajectories of length 3 is given by

$$(B.11a) \quad \mathbb{P}(\zeta = (v_1, v_2, v_3)) = \pi_1 \pi_2^1 \pi_3^2 = \frac{1}{60},$$

$$(B.11b) \quad \mathbb{P}(\zeta = (v_1, v_2, v_4)) = \pi_1 \pi_2^1 \pi_4^2 = \frac{1}{60},$$

$$(B.11c) \quad \mathbb{P}(\zeta = (v_1, v_3, v_1)) = \pi_1 \pi_3^1 \pi_1^3 = \frac{2}{60},$$

$$(B.11d) \quad \mathbb{P}(\zeta = (v_1, v_4, v_3)) = \pi_1 \pi_4^1 \pi_3^4 = \frac{8}{60},$$

$$(B.11e) \quad \mathbb{P}(\zeta = (v_2, v_3, v_1)) = \pi_2 \pi_3^2 \pi_1^3 = \frac{6}{60},$$

$$(B.11f) \quad \mathbb{P}(\zeta = (v_2, v_4, v_3)) = \pi_2 \pi_4^2 \pi_3^4 = \frac{6}{60},$$

$$(B.11g) \quad \mathbb{P}(\zeta = (v_3, v_1, v_2)) = \pi_3 \pi_1^3 \pi_2^1 = \frac{2}{60},$$

$$(B.11h) \quad \mathbb{P}(\zeta = (v_3, v_1, v_3)) = \pi_3 \pi_1^3 \pi_3^1 = \frac{2}{60},$$

$$(B.11i) \quad \mathbb{P}(\zeta = (v_3, v_1, v_4)) = \pi_3 \pi_1^3 \pi_4^1 = \frac{8}{60},$$

$$(B.11j) \quad \mathbb{P}(\zeta = (v_4, v_3, v_1)) = \pi_4 \pi_3^4 \pi_1^3 = \frac{12}{60},$$

$$(B.11k) \quad \mathbb{P}(\zeta = (v_5, v_2, v_3)) = \pi_5 \pi_2^5 \pi_3^2 = \frac{6}{60},$$

$$(B.11l) \quad \mathbb{P}(\zeta = (v_5, v_2, v_4)) = \pi_5 \pi_2^5 \pi_4^2 = \frac{6}{60},$$

where path probabilities satisfy $\mathbb{P}(\zeta[k]) \in [0, 1]$ and $\sum_{k=1}^{12} \mathbb{P}(\zeta[k]) = 1$ for an index $k = 1, \dots, 12$ uniquely associated with the different paths in the support.

Note that the support (all feasible trajectories with nonzero probabilities) involves only consecutive nodes with nonzero transition probabilities. These feasible trajectories are generated by following the connectivity defined by the navigation mesh in [Figure 19](#). Alternatively, one could enumerate all possible permutations of 3 nodes out of the 5 mesh nodes, resulting in ${}^5P_3 = 60$ paths, of which only 12 belong to the policy support. For example, the probability of $\zeta = (v_3, v_2, v_4)$ is given by $\pi_3 \pi_2^3 \pi_4^2 = \frac{1}{2} \times 0 \times \frac{1}{2} = 0$. This of course leads to unneeded waste of computational resources if followed in practical implementations of the policy, for example for sampling.

B.2. Higher-Order Policy. The higher-order policy given by [Definition 3.2](#) employs the conditional transition probability [\(3.12\)](#) to determine which nodes a moving sensor is allowed to transition to. Thus, given a partial path $(\zeta_{n-k}, \dots, \zeta_{n-1})$, the conditional probability of ζ_n is nonzero if the first-order transition probability $\mathbb{P}(\zeta_n | \zeta_{n-i})$ is nonzero for any $i = 1, \dots, k$, where k is the predefined policy order. Note that we assume all lag weights λ_i , $i = 1, \dots, k$ are nonzero.

Distribution support. For clarity, we repeat the same exercise in [Subsection B.2](#) for support generation. Specifically, we generate all paths in the support with length $n = 3$ starting at $\zeta_1 = v_1$. With a partial path containing only one node ($\zeta_1 = v_1$) with policy order $k = 2$, only the first-order transition probabilities are needed to calculate

the conditional transitions probabilities. Thus, similar to the first-order model, the trajectories of length $n = 2$ starting with $\zeta_1 = v_1$ here are

$$(B.12) \quad (\zeta_1 = v_1, \zeta_2) \in \{(v_1, v_2), (v_1, v_3), (v_1, v_4)\}.$$

Now, the third node on the path depends on the last $k = 2$ nodes on the path. If the first-order transition probabilities π_j^i from any of those nodes to a given node ζ_n are nonzero, the node ζ_n can appear next on the path. Let us consider the partial path (v_1, v_2) . Since v_2 can transition to v_3 and v_4 can transition to any of v_2, v_3, v_4 , the next node on the path can be any of v_2, v_3, v_4 . This results in the following possible paths:

$$(B.13) \quad (\zeta_1 = v_1, \zeta_2 = v_2, \zeta_3) \in \{(v_1, v_2, v_2), (v_1, v_2, v_3), (v_1, v_2, v_4)\}.$$

Note that these paths allow transitioning from v_2 to v_1 even though the navigation mesh does not contain an arc (v_2, v_1) . This shows that the proposed higher-order models allow jumps between nodes with joining paths of length up to the policy order k . Similarly, (v_1, v_3) expands to

$$(B.14) \quad (\zeta_1 = v_1, \zeta_2 = v_3, \zeta_3) \in \{(v_1, v_3, v_1), (v_1, v_3, v_2), (v_1, v_3, v_3), (v_1, v_3, v_4)\}$$

and (v_1, v_4) expands to

$$(B.15) \quad (\zeta_1 = v_1, \zeta_2 = v_4, \zeta_3) \{(v_1, v_4, v_2), (v_1, v_4, v_3), (v_1, v_4, v_4)\}.$$

By combining (B.13), (B.14), and (B.15) we obtain all paths of length $n = 3$ in the support starting from $\zeta_1 = v_1$. By following the same strategy with other starting points, the support consisting of 24 trajectories can be constructed.

Probability computations. We show an example of the computations of the path probabilities and leave the rest as an exercise to the reader, since they follow similarly:

$$(B.16) \quad \begin{aligned} \mathbb{P}(\zeta = (v_1, v_2, v_2)) &= \mathbb{P}(v_1) \mathbb{P}(v_2 | v_1) \mathbb{P}(v_2 | v_1, v_2) \\ &\stackrel{(3.14c, 3.14d)}{=} \pi_1 \pi_2^1 \mathbb{P}(\zeta_n = v_2 | \zeta_{n-1} = v_2, \zeta_{n-2} = v_1) \\ &\stackrel{(3.12)}{=} \pi_1 \pi_2^1 (\lambda_1 \mathbb{P}(v_2 | v_2) + \lambda_2 \mathbb{P}(v_2 | v_1)) \\ &\stackrel{(3.12)}{=} \pi_1 \pi_2^1 (\lambda_1 \pi_2^2 + \lambda_2 \pi_2^1) \\ &= \frac{1}{5} \times \frac{1}{6} \left(\frac{2}{3} \times 0 + \frac{1}{3} \times \frac{1}{6} \right) = \frac{1}{540}. \end{aligned}$$

B.3. Generalized Higher-Order Policy.

Distribution support. Here the support consists of 19 trajectories with nonzero probabilities. We follow the same strategy as in Subsection B.3. Expanding a trajectory starting with $\zeta_1 = v_1$ to a path of the same length here is the same as in Subsection B.2. Thus we start by discussing the next node allowed for a partial path (v_1, v_2) under the generalized higher-order policy given by Definition 3.3.

The conditional transition probability (3.16) is used to determine the next nodes allowed on the path starting with $(\zeta_1 = v_1, \zeta_2 = v_2)$. Starting from v_2 , one-step

transition is allowed to either v_3 or v_4 . Starting from v_1 , two-step transition (path consisting of two edges) is allowed to v_1 (via v_3). Thus, given the partial path ($\zeta_1 = v_1, \zeta_2 = v_2$), the conditional transition probability is nonzero only for v_1, v_3, v_4 . Thus the following paths belong to the distribution support:

$$(B.17) \quad (v_1, v_2, v_1), (v_1, v_2, v_3), (v_1, v_2, v_4).$$

We note that the m -step transition probabilities can be obtained, for example, by multiplying the first-step transition probability matrix by itself m times. Thus the two-step transition probability matrix is given by

$$(B.18) \quad \left[\mathbb{P}^{(2)}(v_j | v_i) \right]_{i=1, \dots, 5} = \begin{matrix} & \begin{matrix} v_1 & v_2 & v_3 & v_4 & v_5 \end{matrix} \\ \begin{matrix} v_1 \\ v_2 \\ v_3 \\ v_4 \\ v_5 \end{matrix} & \begin{bmatrix} 2/12 & 0 & 9/12 & 1/12 & 0 \\ 1/2 & 0 & 1/2 & 0 & 0 \\ 0 & 2/12 & 2/12 & 8/12 & 0 \\ 1 & 0 & 0 & 0 & 0 \\ 0 & 0 & 1/2 & 1/2 & 0 \end{bmatrix} \end{matrix},$$

which can be used to enumerate possible 2-step transitions. For example, from the third row we know that there are paths with two edges joining v_3 to and only to each of v_2, v_3, v_4 .

Probability computations. An example of probability computations is given for the path (v_1, v_2, v_1) as follows:

$$(B.19) \quad \begin{aligned} \mathbb{P}(\zeta = (v_1, v_2, v_1)) &= \mathbb{P}(v_1) \mathbb{P}(v_2 | v_1) \mathbb{P}(v_1 | v_1, v_2) \\ &\stackrel{(3.17c, 3.17d)}{=} \pi_1 \pi_2^1 \mathbb{P}(\zeta_n = v_1 | \zeta_{n-1} = v_2, \zeta_{n-2} = v_1) \\ &\stackrel{(3.12)}{=} \pi_1 \pi_2^1 \left(\lambda_1 \mathbb{P}(v_1 | v_2) + \lambda_2 \mathbb{P}^{(2)}(v_1 | v_1) \right) \\ &\stackrel{(3.16, 3.17e)}{=} \frac{1}{5} \times \frac{1}{6} \left(\frac{2}{3} \times 0 + \frac{1}{3} \times \frac{2}{12} \right) = \frac{1}{540}. \end{aligned}$$

The rest of the support—consisting of 19 possible paths—and the full probability distribution under this model can be constructed by following the same steps above.

Note that unlike the case of [Definition 3.2](#), here the trajectory (v_1, v_2, v_2) does not belong to the support of the generalized higher-order policy [Definition 3.3](#). Specifically, $\mathbb{P}(\zeta = (v_1, v_2, v_2)) = 0$ because both $\mathbb{P}(v_2 | v_2) = 0$ and $\mathbb{P}^{(2)}(v_2 | v_1) = 0$, yielding the conditional transition probability $\mathbb{P}(v_2 | v_1, v_2) = 0$.

Appendix C. Additional Numerical Results. Here we provide numerical experiments additional to those presented in [Section 4](#). Specifically, in [Subsection C.1](#) we complement the results presented in [Subsection 4.5](#) with results obtained by employing the fine navigation mesh [Figure 3](#) (right) with $s = 7$ moving sensors, where the starting point of the trajectory is unknown. [Subsection C.2](#) presents results for an experiment in which the starting point of a trajectory is fixed. Finally, in [Subsection C.3](#) we show results for experiments carried out with A- and E-optimality OED criteria, respectively, used to define the utility/objective function.

C.1. Results with Fine Navigation Mesh and 7 Moving Sensors. This section utilizes the same setup used in [Subsection 4.5](#) and replaces the one moving sensor with a group of $s = 7$ moving sensors.

[Figure 20](#) shows the results of [Algorithm 3.3](#) with the first-order policy defined by [Definition 3.1](#). [Figure 21](#) shows the performance of the optimization procedure with the higher-order policy given by [Definition 3.2](#) with order $k = 3$ and $k = 5$, respectively. The resulting optimal initial parameter (first row) and optimal trajectories (second row) under this policy are shown in [Figure 22](#). Similarly, results obtained by employing the generalized higher-order policy given by [Definition 3.3](#) are shown in [Figure 23](#) and [Figure 24](#).

These results support the results in [Subsection 4.5](#) and together show that the proposed approach behaves similarly for different numbers of moving sensors $s \geq 1$. With more sensors, however, the optimization landscape becomes more challenging, with many more designs close to the global optima because of the overlap of the regions containing the moving sensors. This situation is demonstrated by the behavior of the optimization procedure over the early iterations.

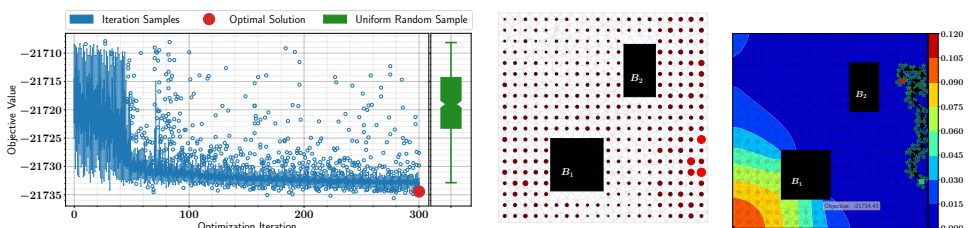


Fig. 20: Results of [Algorithm 3.3](#) with the first-order policy ([Definition 3.1](#)) applied to the fine navigation mesh ([Figure 3](#), right) with trajectory length of $n = 19$ and a group of $s = 7$ moving sensors.

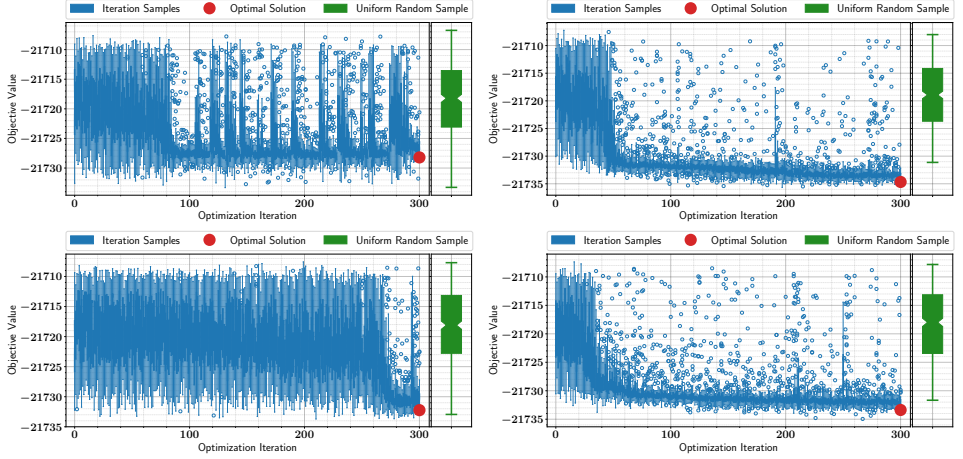


Fig. 21: Results of [Algorithm 3.3](#) with the higher-order policy ([Definition 3.2](#)) applied to the fine navigation mesh ([Figure 3](#), right) with trajectory length of $n = 19$ and $s = 7$ moving sensors. Results are shown for policy order $k = 3$ (first row) and $k = 5$ (second row). The first column shows results with lag weights being calibrated by the optimization procedure, and the second row column shows results with lag weights modeled by [\(3.19\)](#).

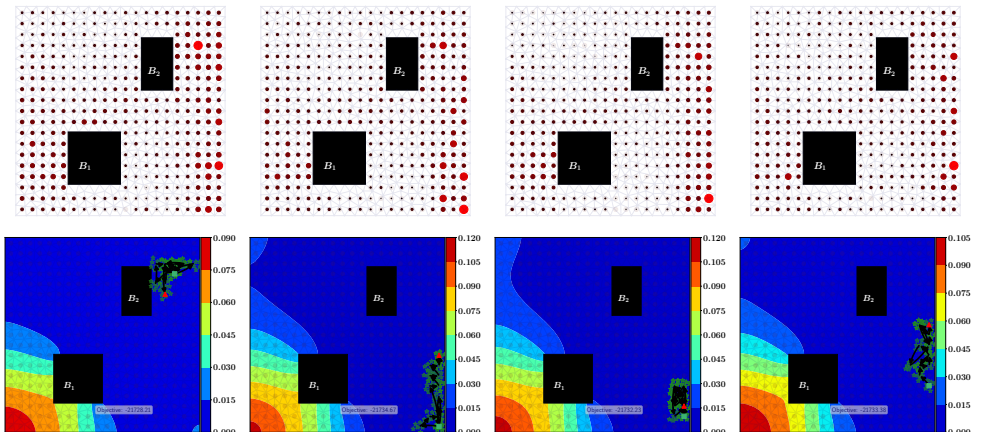


Fig. 22: Optimal initial distribution parameters (top row) and optimal trajectories (bottom row) corresponding to [Figure 21](#). In each row the first two panels match the first row of that figure, followed by panels corresponding to its second row.

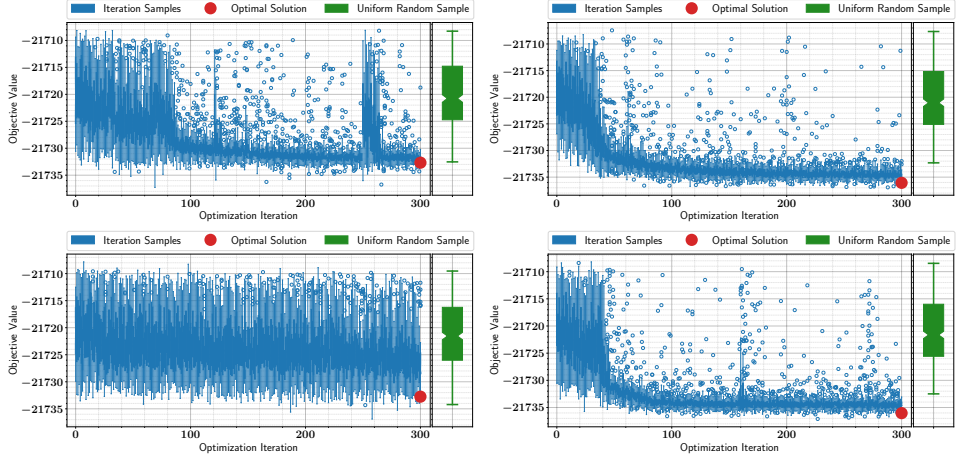


Fig. 23: Results of [Algorithm 3.3](#) with the generalized higher-order policy ([Definition 3.3](#)) applied to the fine navigation mesh ([Figure 3](#), right) with trajectory length of $n = 19$ and $s = 7$ moving sensors. Results are shown for policy order $k = 3$ (first row) and $k = 5$ (second row). The first column shows results with lag weights being calibrated by the optimization procedure, and the second row column shows results with lag weights modeled by [\(3.19\)](#).

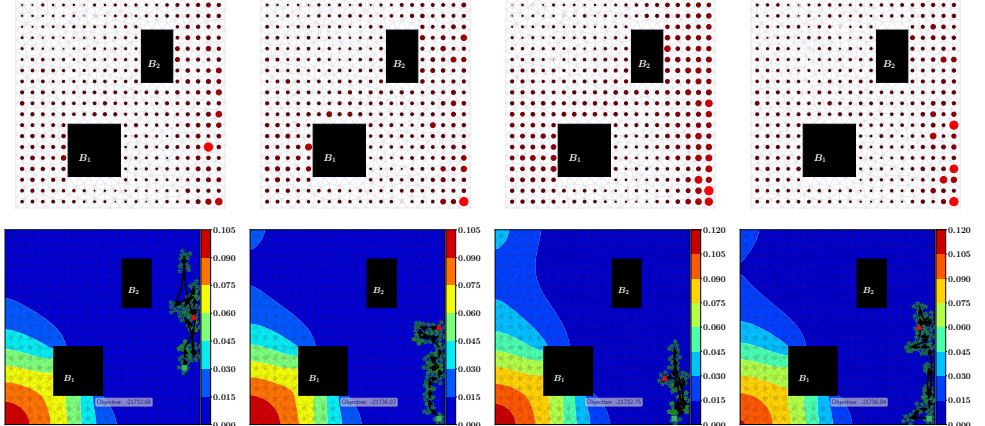


Fig. 24: Optimal initial parameters and trajectories corresponding to [Figure 23](#). In each row, the first two panels match the first row of that figure, followed by panels corresponding to its second row.

C.2. Results with Fine Navigation Mesh and Fixed Starting point.

Here we discuss a different set of experiments in which the path must start at a fixed starting point. Specifically, we enforce the starting point to be at the coordinates $(x, y) = (0.2, 0.7)$ by setting the initial parameter p_i corresponding to that coordinate on the navigation mesh to 1; all other initial parameters are set to 0. Other than the fixed starting point, all settings here are the same as in [Subsection 4.5](#). Results obtained with $s = 1$ moving sensors are given in [Subsection C.2.1](#), and results with $s = 7$ sensors are given in [Subsection C.2.2](#).

C.2.1. Results with 1 Moving Sensor. Figure 25 shows the results of Algorithm 3.3 with the first-order policy defined by Definition 3.1.

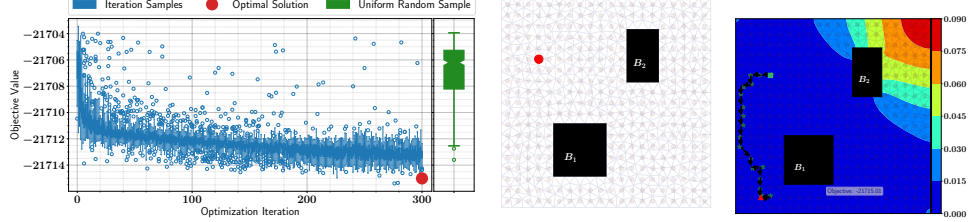


Fig. 25: Results of Algorithm 3.3 with the first-order policy model (Definition 3.1) applied to the fine navigation mesh (Figure 3, right) with the starting point of the trajectory fixed to $(x, y) = (0.2, 0.7)$. Trajectory length is $n = 19$, and the sensor size is $s = 1$.

Figure 26 shows the performance of the optimization procedure with the higher-order policy given by Definition 3.2 with order $k = 3$ and $k = 5$, respectively. The resulting optimal initial parameter (first row) and optimal trajectories (second row) are shown in Figure 27.

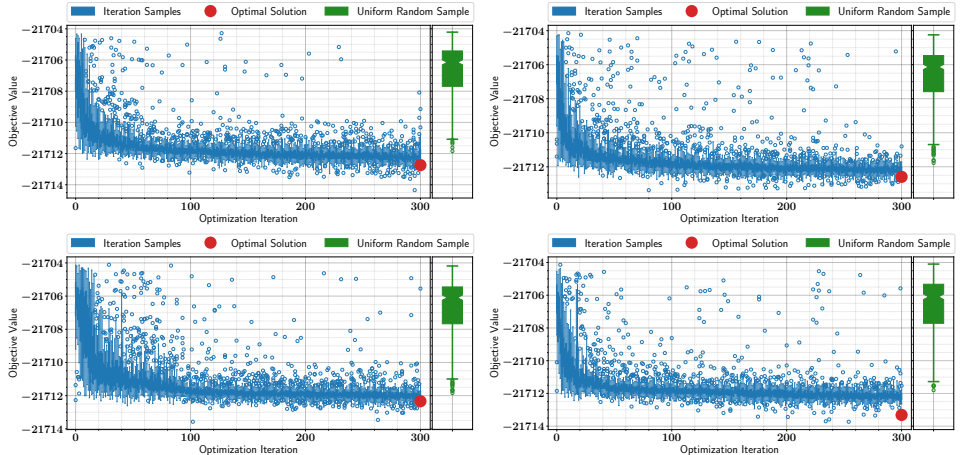


Fig. 26: Results of Algorithm 3.3 with the higher-order policy model (Definition 3.2) applied to the fine navigation mesh (Figure 3, right) with the starting point of the trajectory fixed to $(x, y) = (0.2, 0.7)$. Trajectory length is $n = 19$, and the sensor size is $s = 1$. The policy order is set to $k = 3$ (first row) and to $k = 5$ (second row). The first column shows results with lag weights being optimized, and the second column shows results with lag weights modeled by (3.19).

Similarly, results obtained by the policy given by Definition 3.2 are shown in Figure 28 and Figure 29.

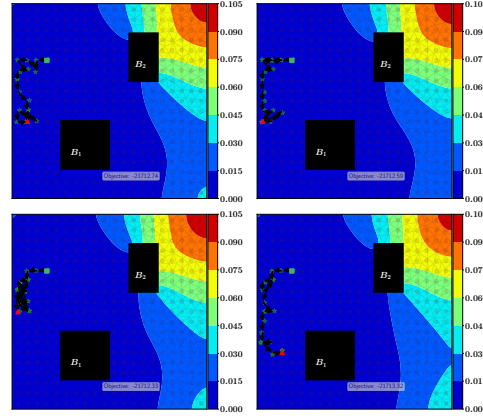


Fig. 27: Optimal trajectories corresponding to results shown in Figure 26.

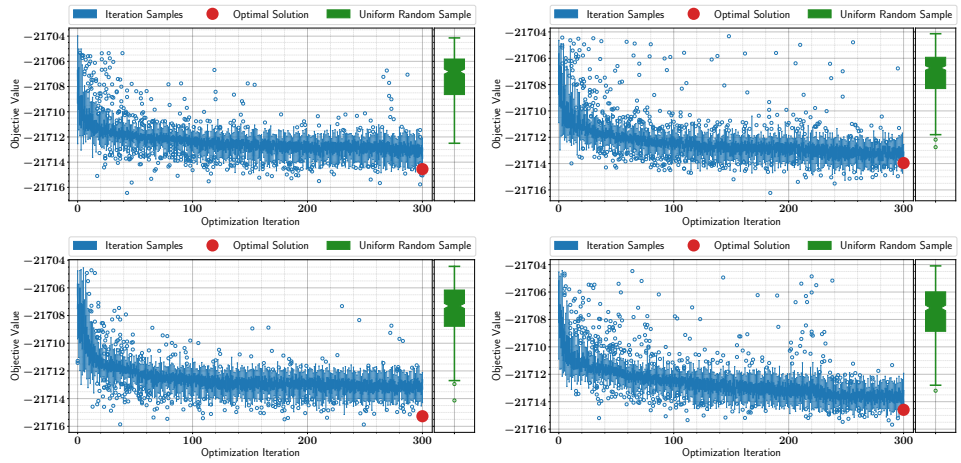


Fig. 28: Similar to Figure 26. Here the generalized higher-order policy (Definition 3.3) is used.

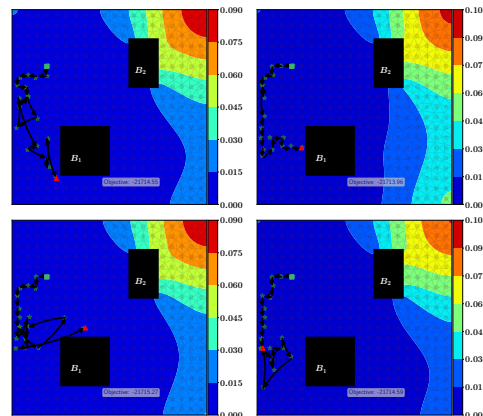


Fig. 29: Optimal trajectories corresponding to results shown in Figure 28.

C.2.2. Results with 7 Moving Sensors. This case simulates $s = 7$ sensors (e.g., drones) moving together.

Figure 30 shows the results of Algorithm 3.3 with the first-order policy defined by Definition 3.1.

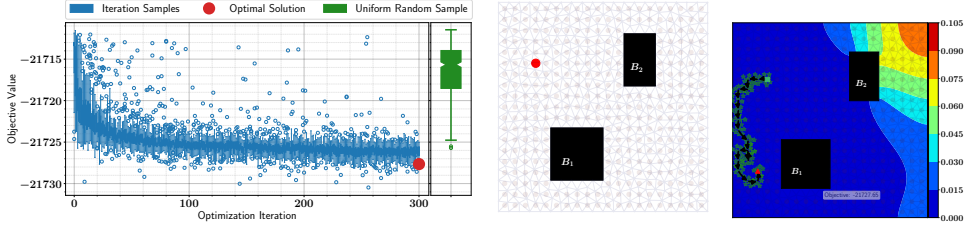


Fig. 30: Results of Algorithm 3.3 with the first-order policy model (Definition 3.1) applied to the fine navigation mesh (Figure 3, right) with the starting point of the trajectory fixed to $(x, y) = (0.2, 0.7)$. Trajectory length is $n = 19$, and the sensor size is $s = 7$.

Figure 31 shows the performance of the optimization procedure with the higher-order policy given by Definition 3.2 with order $k = 3$ and $k = 5$, respectively. The resulting optimal initial parameter (first row) and optimal trajectories (second row) are shown in Figure 32.

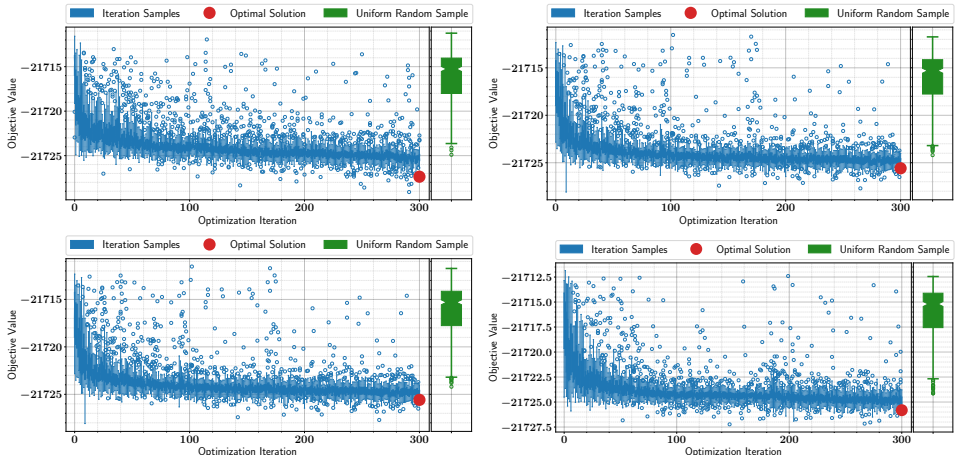


Fig. 31: Results of Algorithm 3.3 applied to the fine navigation mesh (Figure 3, right) with the starting point of the trajectory fixed to $(x, y) = (0.2, 0.7)$. Trajectory length is $n = 19$, and the sensor size is $s = 7$. Here the higher-order policy (Definition 3.2) is used with orders $k = 3$ (first row) and $k = 5$ (second row). The first column shows results with lag weights being optimized, and the second column shows results with lag weights modeled by (3.19).

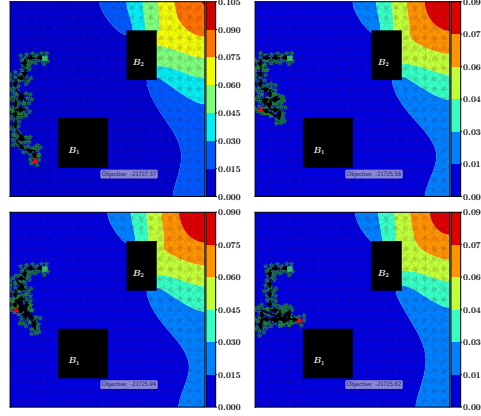


Fig. 32: Optimal trajectories corresponding to results shown in Figure 31.

Similarly, results obtained by the policy given by Definition 3.3 are shown in Figure 33 and Figure 34.

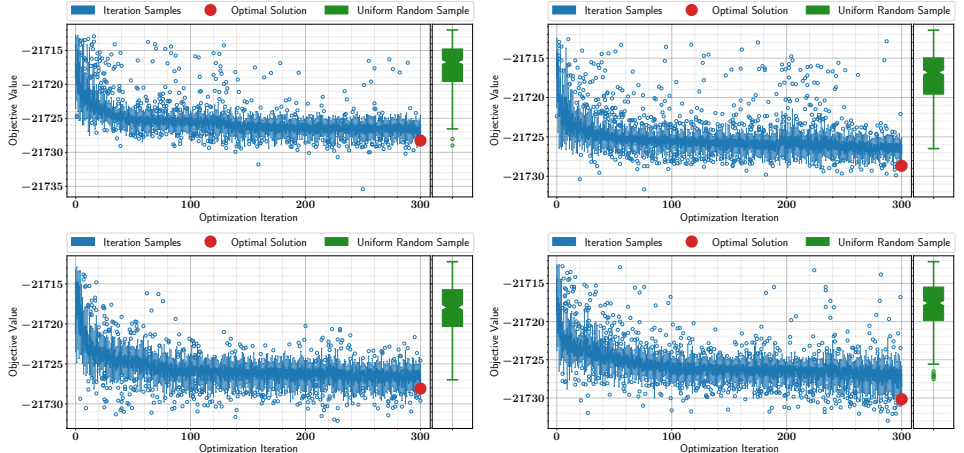


Fig. 33: Results of Algorithm 3.3 with the generalized higher-order policy model (Definition 3.3) applied to the fine navigation mesh (Figure 3, right) with the starting point of the trajectory fixed to $(x, y) = (0.2, 0.7)$. Trajectory length is $n = 19$, and the sensor size is $s = 7$. Here the generalized higher-order policy (Definition 3.3) is used with orders $k = 3$ (first row) and $k = 5$ (second row). The first column shows results with lag weights being optimized, and the second column shows results with lag weights modeled by (3.19).

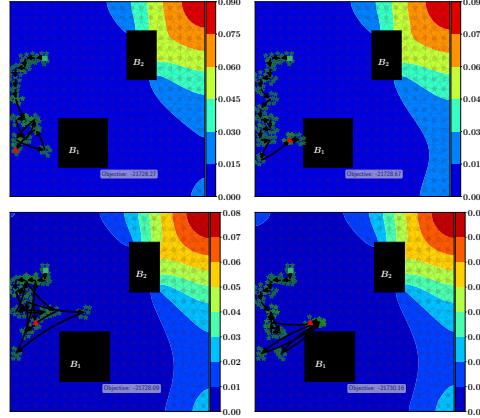


Fig. 34: Optimal trajectories corresponding to results shown in Figure 33.

The results displayed in Subsection C.2.2 for $s = 7$ moving sensors are consistent with the results obtained with $s = 1$ moving sensor in Subsection C.2.1, and with the coarse mesh experiment discussed in Subsection 4.3.

C.3. Results with A- and E-Optimality Criteria. In this section we show a partial set of results obtained by using optimality criteria other than the D-optimality used primarily in the numerical experiments. Specifically, we present in Subsection C.3.1 results obtained by using the A-optimality (trace/average of the posterior variances) criterion. Subsection C.3.2 presents results obtained by employing the E-optimality (eigenvalue) criterion.

Similar to Subsection 4.5, this experiment employs the fine navigation mesh Figure 3 (right). The trajectory length is set to $n = 19$ nodes (18 edges), and the observation frequency is set to $f = 1$. The number of sensors is set to $s = 1$ and $s = 7$, respectively, and is stated clearly in each figure. First we show results with the starting point of the path restricted to the coordinates $(x, y) = (0.2, 0.7)$, and then we allow the trajectory to start anywhere in the domain, allowing the starting point to be optimized as well.

For clarity, we show results obtained only by using the first-order policy (Definition 3.1). We note that the same behavior as in the case of D-optimality is observed here for higher-order policies in comparison with the first-order policy.

C.3.1. Results with A-Optimality Criterion. For the A-optimality, the objective is to minimize the sum of posterior variances. The probabilistic OED optimization (Problem 3.2) in this case takes the form

$$(C.1) \quad \mathbf{p}^{\text{opt}} \in \arg \min_{\zeta \sim \mathbb{P}(\zeta | \mathbf{p})} \mathbb{E}_{\zeta \sim \mathbb{P}(\zeta | \mathbf{p})} [\mathcal{U}(\zeta)]; \quad \mathcal{U}(\zeta) := \text{Tr}(\mathbf{\Gamma}_{\text{post}}(\zeta)),$$

where $\mathbf{\Gamma}_{\text{post}}(\zeta)$ is the posterior covariance matrix (4.2).

Results with fixed starting point. Figure 35 shows the results of Algorithm 3.3 with the first-order policy defined by Definition 3.1 and with the number of sensors set to $s = 1$. Results obtained with $s = 7$ moving sensors are shown in Figure 36.

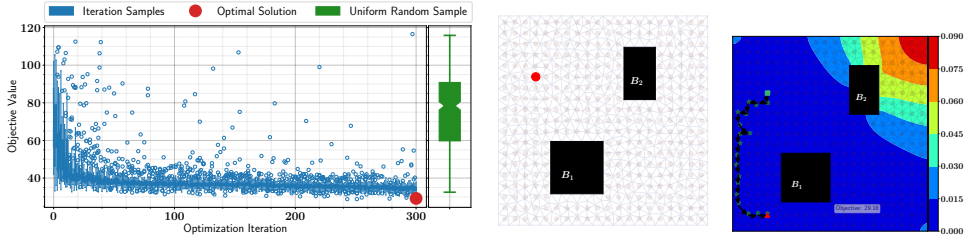


Fig. 35: Results of Algorithm 3.3 with the first-order policy model (Definition 3.1) applied to the fine navigation mesh (Figure 3, right) with the starting point of the trajectory fixed to $(x, y) = (0.2, 0.7)$. The optimality criterion used is the A-optimality, that is, the trace of the posterior covariance matrix. The number of sensors is set to $s = 1$, the observation frequency is $f = 1$, and the trajectory length is $n = 19$.

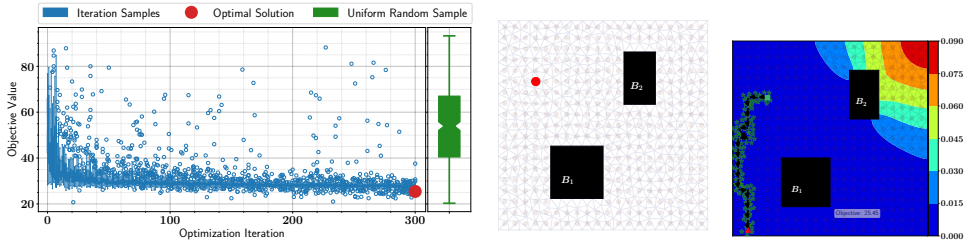


Fig. 36: Similar to Figure 35. Here the number of moving sensors is set to $s = 7$.

Results with unspecified starting point. Figure 37 shows the results of Algorithm 3.3 with the first-order policy defined by Definition 3.1 and with number of sensors set to $s = 1$. Figure 38 shows the results obtained by setting the number of moving sensors to $s = 7$.

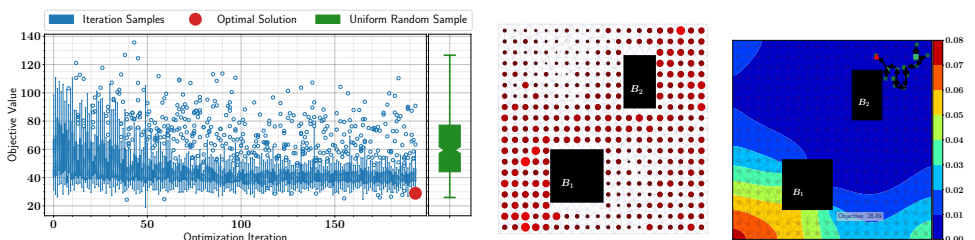


Fig. 37: Results of Algorithm 3.3 with the first-order policy model (Definition 3.1) applied to the fine navigation mesh (Figure 3, right) with unspecified starting point of the trajectory. The optimality criterion used is the A-optimality, that is, the trace of the posterior covariance matrix. The number of sensors is set to $s = 1$, the observation frequency is $f = 1$, and the trajectory length is $n = 19$.

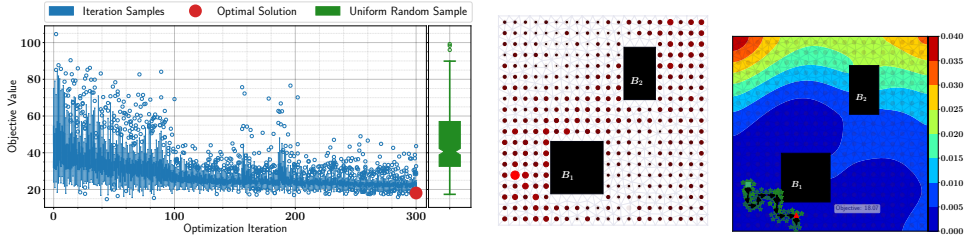


Fig. 38: Similar to Figure 37. Here the number of moving sensors is set to $s = 7$.

C.3.2. Results with E-Optimality Criterion. For the E-optimality, the objective is to minimize the maximum eigenvalue of posterior covariance matrix, that is, $\lambda_{\max}(\mathbf{\Gamma}_{\text{post}}(\zeta))$. This function (maximum eigenvalue) is not typically used in classical model-based OED and in general in gradient-based optimization because of challenges in developing its derivative [2, 35]. In these approaches the derivative of the utility function \mathcal{U} with respect to the design ζ is needed, and thus the discrete design is relaxed to allow values in the real-valued space. The optimal relaxed design is then rounded to retrieve an estimate of the solution of the original discrete optimization problem; see, for example, [7].

Since the proposed algorithms treat the objective as a black box, this function can be used in the proposed framework out of the box without the need for such complications. The probabilistic OED optimization (Problem 3.2) in this case takes the form

$$(C.2) \quad \mathbf{p}^{\text{opt}} \in \arg \min_{\zeta \sim \mathbb{P}(\zeta | \mathbf{p})} \mathbb{E}_{\zeta \sim \mathbb{P}(\zeta | \mathbf{p})} [\mathcal{U}(\zeta)]; \quad \mathcal{U}(\zeta) := \lambda_{\max}(\mathbf{\Gamma}_{\text{post}}(\zeta)),$$

where $\mathbf{\Gamma}_{\text{post}}(\zeta)$ is the posterior covariance matrix (4.2).

Results with fixed starting point. Figure 39 shows the results of Algorithm 3.3 with the first-order policy defined by Definition 3.1 and with the number of sensors set to $s = 1$. Results obtained with $s = 7$ moving sensors are shown in Figure 40

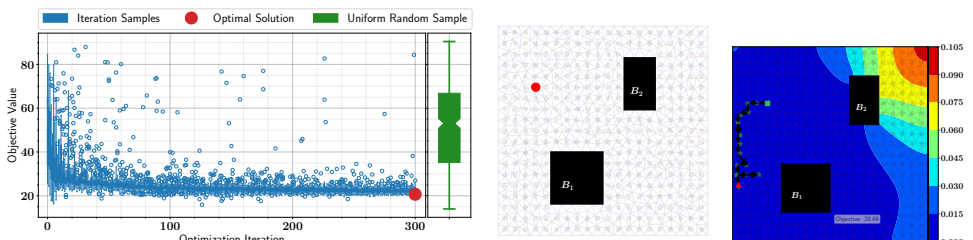


Fig. 39: Results of Algorithm 3.3 with the first-order policy model (Definition 3.1) applied to the fine navigation mesh (Figure 3, right) with the starting point of the trajectory fixed to $(x, y) = (0.2, 0.7)$. The optimality criterion used is the E-optimality, that is, the trace of the posterior covariance matrix. The number of sensors is set to $s = 1$, the observation frequency is $f = 1$, and the trajectory length is $n = 19$.

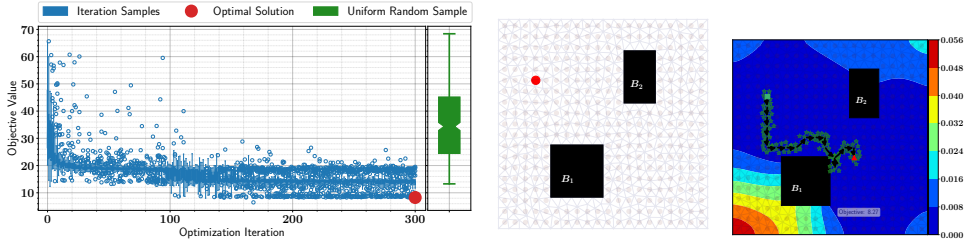


Fig. 40: Similar to Figure 39. Here the number of moving sensors is set to $s = 7$.

Results with unspecified starting point. Figure 41 shows the results of Algorithm 3.3 with the first-order policy defined by Definition 3.1 and with the number of sensors set to $s = 1$. Figure 42 shows the results obtained by setting the number of moving sensors to $s = 7$.

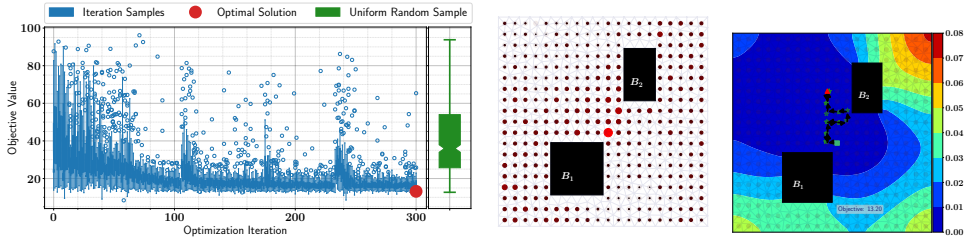


Fig. 41: Results of Algorithm 3.3 with the first-order policy model (Definition 3.1) applied to the fine navigation mesh (Figure 3, right) with unspecified starting point of the trajectory. The optimality criterion used is the E-optimality, that is, the maximum eigenvalue of the posterior covariance matrix. The number of sensors is set to $s = 1$, the observation frequency is $f = 1$, and the trajectory length is $n = 19$.

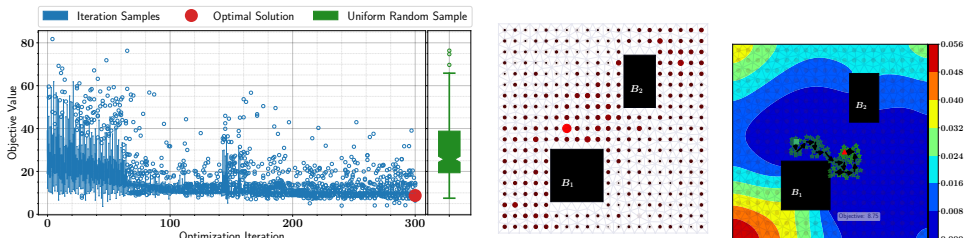


Fig. 42: Similar to Figure 41. Here the number of moving sensors is set to $s = 7$.

The results presented here show that the optimization procedure behaves similarly for various choices of the optimality criterion and are thus consistent with the experiment carried out with the D-optimality objective. The resulting optimal trajectories, however, are potentially different in shape, exploring relatively different parts of the space. Nevertheless, for all choices of the criteria here, the optimal trajectory falls in regions with minimum activity because these locations are associated with minimum uncertainty due to the way the synthetic data and noise covariance matrix is constructed. The choice of the utility function, however, is independent from the proposed approach and should be the user's choice.

For all the utility functions employed here, overall the optimizer quickly reduces the average value of the objective/utility function, converging to the tail of the utility function distribution. This enables exploring the design space near global optima. Reaching the global optimal value, however, is not guaranteed.

Acknowledgments. Thanks to Alen Alexanderian (NCSU) for discussion and feedback, and to Gail Piper (ANL) for editing this manuscript.

REFERENCES

- [1] A. ALEXANDERIAN, *Optimal experimental design for infinite-dimensional Bayesian inverse problems governed by PDEs: A review*, Inverse Problems, 37 (2021), p. 043001.
- [2] A. L. ANDREW, K.-W. E. CHU, AND P. LANCASTER, *Derivatives of eigenvalues and eigenvectors of matrix functions*, SIAM Journal on Matrix Analysis and Applications, 14 (1993), pp. 903–926.
- [3] M. ASCH, M. BOCQUET, AND M. NODET, *Data assimilation: methods, algorithms, and applications*, SIAM, 2016.
- [4] A. ATTIA, *Probabilistic approach to black-box binary optimization with budget constraints: Application to sensor placement*, arXiv preprint arXiv:2406.05830, (2024).
- [5] A. ATTIA, *PyOED: An extensible suite for data assimilation and model-based optimal experimental design*. <https://gitlab.com/ahmedattia/pyoed>, <https://web.cels.anl.gov/~aattia/pyoed/>, 2026.
- [6] A. ATTIA, A. ALEXANDERIAN, AND A. K. SAIBABA, *Goal-oriented optimal design of experiments for large-scale Bayesian linear inverse problems*, Inverse Problems, 34 (2018), p. 095009.
- [7] A. ATTIA AND E. CONSTANTINESCU, *Optimal experimental design for inverse problems in the presence of observation correlations*, SIAM Journal on Scientific Computing, 44 (2022), pp. A2808–A2842.
- [8] A. ATTIA, S. LEYFFER, AND T. S. MUNSON, *Stochastic learning approach for binary optimization: Application to Bayesian optimal design of experiments*, SIAM Journal on Scientific Computing, 44 (2022), pp. B395–B427.
- [9] A. ATTIA, S. LEYFFER, AND T. S. MUNSON, *Robust α -optimal experimental design for sensor placement in Bayesian linear inverse problems*, SIAM/ASA Journal on Uncertainty Quantification, 13 (2025), pp. 744–774.
- [10] A. ATTIA, V. RAO, AND A. SANDU, *A hybrid Monte-Carlo sampling smoother for four-dimensional data assimilation*, International Journal for Numerical Methods in Fluids, 83 (2017), pp. 90–112.
- [11] A. ATTIA, R. ŠTEFĀNESCU, AND A. SANDU, *The reduced-order hybrid Monte Carlo sampling smoother*, International Journal for Numerical Methods in Fluids, 83 (2017), pp. 28–51.
- [12] D. P. BERTSEKAS AND J. N. TSITSIKLIS, *Neuro-dynamic programming: an overview*, in Proceedings of 1995 34th IEEE Conference on Decision and Control, vol. 1, IEEE, 1995, pp. 560–564.
- [13] M. BRANDAO, A. COLES, AND D. MAGAZZENI, *Explaining path plan optimality: Fast explanation methods for navigation meshes using full and incremental inverse optimization*, in Proceedings of the International Conference on Automated Planning and Scheduling, vol. 31, 2021, pp. 56–64.
- [14] W. K. CHING, E. S. FUNG, AND M. K. NG, *Higher-order Markov chain models for categorical data sequences*, Naval Research Logistics (NRL), 51 (2004), pp. 557–574.
- [15] W.-K. CHING AND M. K. NG, *Markov chains: models, algorithms and applications*, Springer, 2006.
- [16] W.-K. CHING, M. K. NG, AND E. S. FUNG, *Higher-order multivariate Markov chains and their applications*, Linear Algebra and its Applications, 428 (2008), pp. 492–507.
- [17] H. CHOSET, K. M. LYNCH, S. HUTCHINSON, G. A. KANTOR, AND W. BURGARD, *Principles of robot motion: theory, algorithms, and implementations*, MIT Press, 2005.
- [18] A. CHOWDHARY, S. E. AHMED, AND A. ATTIA, *PyOED: An extensible suite for data assimilation and model-constrained optimal design of experiments*, ACM Transactions on Mathematical Software, 50 (2025), pp. 1–22.
- [19] V. FEDOROV AND J. LEE, *Design of experiments in statistics*, in Handbook of Semidefinite Programming, R. S. H. Wolkowicz and L. Vandenberghe, eds., vol. 27 of Internat. Ser. Oper. Res. Management Sci., Kluwer Acad. Publ., Boston, MA, 2000, pp. 511–532.
- [20] V. V. FEDOROV, *Theory of optimal experiments*, Elsevier, 2013.

- [21] A. GASPERETTO, P. BOSCAROL, A. LANZUTTI, AND R. VIDONI, *Path planning and trajectory planning algorithms: A general overview*, Motion and Operation Planning of Robotic Systems: Background and Practical Approaches, (2015), pp. 3–27.
- [22] P. E. HART, N. J. NILSSON, AND B. RAPHAEL, *A formal basis for the heuristic determination of minimum cost paths*, IEEE Transactions on Systems Science and Cybernetics, 4 (1968), pp. 100–107.
- [23] X. HUAN, J. JAGALUR, AND Y. MARZOUK, *Optimal experimental design: Formulations and computations*, Acta Numerica, 33 (2024), pp. 715–840.
- [24] X. HUAN AND Y. MARZOUK, *Gradient-based stochastic optimization methods in Bayesian experimental design*, International Journal for Uncertainty Quantification, 4 (2014).
- [25] K. KARUR, N. SHARMA, C. DHARMATTI, AND J. E. SIEGEL, *A survey of path planning algorithms for mobile robots*, Vehicles, 3 (2021), pp. 448–468.
- [26] J.-C. LATOMBE, *Robot motion planning*, vol. 124, Springer Science & Business Media, 2012.
- [27] S. M. LAVALLE, *Planning algorithms*, Cambridge University Press, 2006.
- [28] K. LAW, A. STUART, AND K. ZYGALAKIS, *Data assimilation*, Cham, Switzerland: Springer, 214 (2015), p. 52.
- [29] S. LIN, A. LIU, J. WANG, AND X. KONG, *A review of path-planning approaches for multiple mobile robots*, Machines, 10 (2022), p. 773.
- [30] A. PÁZMAN, *Foundations of optimum experimental design*, D. Reidel Publishing Co., 1986.
- [31] N. PETRA AND G. STADLER, *Model variational inverse problems governed by partial differential equations*, Tech. Report 11-05, The Institute for Computational Engineering and Sciences, The University of Texas at Austin, 2011.
- [32] F. PUKELSHEIM, *Optimal design of experiments*, John Wiley & Sons, New-York, 1993.
- [33] E. RAFAJŁOWICZ, *Optimum choice of moving sensor trajectories for distributed-parameter system identification*, International Journal of Control, 43 (1986), pp. 1441–1451.
- [34] A. E. RAFTERY, *A model for high-order Markov chains*, Journal of the Royal Statistical Society Series B: Statistical Methodology, 47 (1985), pp. 528–539.
- [35] L. C. ROGERS, *Derivatives of eigenvalues and eigenvectors*, AIAA Journal, 8 (1970), pp. 943–944.
- [36] A. M. STUART, *Inverse problems: a Bayesian perspective*, Acta Numerica, 19 (2010), pp. 451–559.
- [37] A. SUNTER, *Solutions to the problem of unequal probability sampling without replacement*, International Statistical Review/Revue Internationale de Statistique, (1986), pp. 33–50.
- [38] C. TRICAUD, M. PATAN, U. DARIUSZ, AND Y. Q. CHEN, *D-optimal trajectory design of heterogeneous mobile sensors for parameter estimation of distributed systems*, in 2008 American Control Conference, IEEE, 2008, pp. 663–668.
- [39] D. UCIŃSKI, *Optimal measurement methods for distributed parameter system identification*, CRC Press, Boca Raton, 2005.
- [40] H. P. WYNN, *Results in the theory and construction of D-optimum experimental designs*, Journal of the Royal Statistical Society Series B: Statistical Methodology, 34 (1972), pp. 133–147.

The submitted manuscript has been created by UChicago Argonne, LLC, Operator of Argonne National Laboratory (“Argonne”). Argonne, a U.S. Department of Energy Office of Science laboratory, is operated under Contract No. DE-AC02-06CH11357. The U.S. Government retains for itself, and others acting on its behalf, a paid-up nonexclusive, irrevocable worldwide license in said article to reproduce, prepare derivative works, distribute copies to the public, and perform publicly and display publicly, by or on behalf of the Government. The Department of Energy will provide public access to these results of federally sponsored research in accordance with the DOE Public Access Plan. <http://energy.gov/downloads/doe-public-access-plan>.